



Global studies on a continuous planar piecewise linear differential system with three zones

Man Jia · Youfeng Su  · Hebai Chen

Received: 18 June 2022 / Accepted: 12 October 2022 / Published online: 20 October 2022
© The Author(s), under exclusive licence to Springer Nature B.V. 2022

Abstract This paper is concerned with the global dynamics of a continuous planar piecewise linear differential system with three zones, where the dynamic of the one of the exterior linear zones is saddle and the remaining one is anti-saddle. We give all global phase portraits in the Poincaré disc and the complete bifurcation diagram including boundary equilibrium bifurcation curves, degenerate boundary equilibrium bifurcation curves, homoclinic bifurcation curves and double limit cycle bifurcation curves. Its application in a second-order memristor oscillator is shown. Finally, some numerical phase portraits are demonstrated to illustrate our theoretical results.

Keywords Piecewise linear system · Global phase portrait · Bifurcation · Limit cycle · Homoclinic loop

M. Jia
Center for Discrete Mathematics, Fuzhou University,
Fuzhou 350116, Fujian, People's Republic of China

M. Jia
School of Mathematics and Statistics, Fuzhou University,
Fuzhou 350116, Fujian, People's Republic of China
e-mail: jiaman9305@163.com

Y. Su (✉)
College of Computer and Date Science, Fuzhou University,
Fuzhou 350116, Fujian, People's Republic of China
e-mail: yfsu@fzu.edu.cn

H. Chen
School of Mathematics and Statistics, HNP-LAMA,
Central South University, Changsha 410083, Hunan,
People's Republic of China
e-mail: chen_hebai@csu.edu.cn

Mathematics Subject Classification 34C07 · 34C23 · 34C37 · 34K18

1 Introduction

In recent years, there has been tremendous interest in developing piecewise linear differential systems, see [1, 3–6, 21, 23, 26, 28, 30, 35, 39] and references therein. In applied science and engineering, piecewise linear differential systems can model a large number of nonlinear problems. Particularly, the global dynamics of some nonlinear models can be approximated by piecewise linear differential systems, such as some memristor oscillators (see [7–10, 18, 24, 31, 32, 36]) and FitzHugh–Nagumo system (see [33, 34, 37]). Although piecewise linear differential systems seem simple, they have rich and complex dynamics even with the low-dimensional spaces. Moreover, piecewise linear differential systems have not only all the dynamics of general smooth nonlinear systems (such as limit cycles, homoclinic loops, heteroclinic loops, strange attractors and so on), but also special dynamical behaviors (such as jump bifurcation, grazing bifurcation, sliding bifurcation, singular continuous systems and so on), see [18, 19] and references therein.

This paper focuses on planar piecewise linear differential systems. There are two types of these systems: “continuous” and “discontinuous”. For continuous planar piecewise linear (CPWL) differential systems with two linear zones separated by a straight line,

the study of their dynamics has been well considered. For such system the existence of at most one limit cycle was given in [20]. A necessary and sufficient condition of the existence of limit cycles was proven in [31]. Global phase portraits in the Poincaré disc with single equilibrium point were shown in [25]. A lot of effort has been devoted to characterize the global dynamics of CPWL differential systems with three linear zones separated by two parallel straight lines, see [8–14, 19, 21, 27, 29, 31, 32, 35] and references therein. However, there are still many cases that have not been studied.

In this paper, we consider a CPWL differential system with three linear zones in Liénard form as follows

$$\frac{dx}{dt} = F(x) - y, \quad \frac{dy}{dt} = g(x) - \alpha, \tag{1}$$

where

$$F(x) = \begin{cases} t_r(x - 1) + t_c, & \text{if } x > 1, \\ t_c x, & \text{if } -1 \leq x \leq 1, \\ t_l(x + 1) - t_c, & \text{if } x < -1, \end{cases}$$

and

$$g(x) = \begin{cases} d_r(x - 1) + d_c, & \text{if } x > 1, \\ d_c x, & \text{if } -1 \leq x \leq 1, \\ d_l(x + 1) - d_c, & \text{if } x < -1. \end{cases}$$

The plane \mathbb{R}^2 is divided into three open linear zones

$$\begin{aligned} \mathcal{S}_l &:= \{(x, y) \in \mathbb{R}^2 \mid x < -1\}, \\ \mathcal{S}_c &:= \{(x, y) \in \mathbb{R}^2 \mid -1 < x < 1\}, \\ \mathcal{S}_r &:= \{(x, y) \in \mathbb{R}^2 \mid x > 1\} \end{aligned}$$

by two parallel straight lines $\Gamma_l := \{(x, y) \in \mathbb{R}^2 \mid x = -1\}$ and $\Gamma_r := \{(x, y) \in \mathbb{R}^2 \mid x = 1\}$. Note that system (1) is analytic in $\mathbb{R}^2 \setminus \{\Gamma_l \cup \Gamma_r\}$ and Lipschitz continuous in \mathbb{R}^2 . Thus the classical theorems on existence, uniqueness and continuity of solutions all hold for system (1) with respect to initial conditions and parameters, see [31].

In particular, when system (1) is symmetric with respect to the origin ($t_r = t_l$, $d_r = d_l$ and $\alpha = 0$), the global dynamics of system (1) have been studied in [8, 9, 21, 27, 29] and references therein. When the determinant for the Jacobian matrix of its central zone vanishes ($d_c = 0$), we call system (1) with three zones *degenerate planar piecewise linear differential systems*. The study of the global dynamics of such systems has been completely investigated when $t_r t_l < 0$, $d_r > 0$ and $d_l > 0$, see [11, 14, 19]. The conditions of

$d_r > 0$ and $d_l > 0$ mean that the dynamics of left and right linear zones of system (1) are anti-saddles. For the case $d_r > 0$, $d_c \neq 0$ and $d_l > 0$, there are many results about global dynamics for system (1), such as the N -shaped curve ($t_r t_l > 0$) (see [12, 31, 35]) and the U -shaped curve ($t_r t_l < 0$) (see [10, 31, 32]). However, there is a gap that no research concerns the global dynamics of system (1) with three linear zones assuming $d_r d_l < 0$. The condition $d_r d_l < 0$ implies that the dynamic of one of the left and right linear zones of system (1) is saddle, and the remaining one is anti-saddle. System (1) with $d_r d_l < 0$ has not only the same dynamics of system (1) with $d_r > 0$, $d_l > 0$ (for example, the existence of exactly two limit cycles), but also special dynamical behaviors (for example, the coexistence of limit cycle and homoclinic loop). This shows that the dynamics of system (1) with condition $d_r d_l < 0$ is more complex than the case $d_r > 0$, $d_l > 0$, even assuming the other conditions are the same. The main purpose of this paper is to study system (1) whose parameters belong to the following region:

$$\mathcal{G} := \{(t_r, t_l, d_r, d_c, d_l) \in \mathbb{R}^5 \mid t_r t_l > 0, d_r d_l < 0\}.$$

For simplicity, \mathcal{G} can be divided into the following four parameter regions:

$$\begin{aligned} \mathcal{G}_1 &:= \{(t_r, t_l, d_r, d_c, d_l) \in \mathbb{R}^5 \mid t_r > 0, \\ &\quad t_l > 0, d_r > 0, d_l < 0\}, \\ \mathcal{G}_2 &:= \{(t_r, t_l, d_r, d_c, d_l) \in \mathbb{R}^5 \mid t_r > 0, \\ &\quad t_l > 0, d_r < 0, d_l > 0\}, \\ \mathcal{G}_3 &:= \{(t_r, t_l, d_r, d_c, d_l) \in \mathbb{R}^5 \mid t_r < 0, \\ &\quad t_l < 0, d_r > 0, d_l < 0\}, \\ \mathcal{G}_4 &:= \{(t_r, t_l, d_r, d_c, d_l) \in \mathbb{R}^5 \mid t_r < 0, \\ &\quad t_l < 0, d_r < 0, d_l > 0\}. \end{aligned}$$

Using transformation

$$\begin{aligned} &(x, y, t, t_r, t_c, t_l, d_r, d_c, d_l, \alpha) \\ &\quad \rightarrow (-x, -y, t, t_l, t_c, t_r, d_l, d_c, d_r, -\alpha) \\ &(\text{resp. } (x, y, t, t_r, t_c, t_l, d_r, d_c, d_l, \alpha) \\ &\quad \rightarrow (x, -y, -t, -t_r, -t_c, -t_l, d_r, d_c, d_l, \alpha); \\ &(x, y, t, t_r, t_c, t_l, d_r, d_c, d_l, \alpha) \\ &\quad \rightarrow (-x, y, -t, -t_l, -t_c, -t_r, d_l, d_c, d_r, -\alpha)) \end{aligned}$$

the vector field $(F(x) - y, g(x) - \alpha)$ of system (1) is invariant and the parameter region \mathcal{G}_2 (resp. \mathcal{G}_3 ; \mathcal{G}_4)

can be changed into the parameter region \mathcal{G}_1 . Thus, it suffices to discuss system (1) in the parameter region \mathcal{G}_1 . Since the value of the determinant for the Jacobian matrix of central zone of system (1) is d_c , the condition $d_c < 0$ (resp. $d_c > 0$) means that the dynamic of its central zone is saddle (resp. anti-saddle). And the condition $d_c = 0$ implies that system (1) has a singular continuum. Therefore, system (1) will be studied in three cases $d_c < 0$, $d_c = 0$ and $d_c > 0$. Although the qualitative property of equilibrium point at infinity is the same for system (1) in the cases $d_c > 0$ and $d_c \leq 0$, the results for the finite equilibrium point are utterly different. Naturally, the global phase portraits and bifurcations of system (1) with $d_c > 0$ are completely different from those of system (1) with $d_c \leq 0$. Owing to the length of this article, we consider two cases $d_c = 0$ and $d_c < 0$ in \mathcal{G}_1 . For the case $d_c > 0$ in \mathcal{G}_1 , we will study the global dynamics of system (1) in a future paper.

An outline of this paper is as follows. We devote Sect. 2 to a show of the main results, i.e., the bifurcation diagram in the αt_c -plane and global phase portraits in the Poincaré disc of system (1) as parameters belong to the region \mathcal{G}_1 for $d_c \leq 0$. Its application in a second-order memristor oscillator is shown in Sect. 3. We give the local dynamics of system (1) in Sect. 4. The study of limit cycles and homoclinic loops of system (1) is presented in Sect. 5. Proofs of the main results are given in Sect. 6. Numerical phase portraits are then presented in Sect. 7, illustrating the analytical results. Finally, some concluding remarks of this paper are presented in Sect. 8.

2 Main results

In this paper, we consider the cases $d_c = 0$ and $d_c < 0$ for system (1) in \mathcal{G}_1 . The condition $t_r^2 - 4d_r < 0$ (resp. $= 0; > 0$) implies that the dynamic of right linear zone of system (1) is a focus (resp. improper node; bidirectional node) (see Lemma 4.1 for more descriptions). Moreover, system (1) has the different qualitative properties of equilibrium point at infinity for the different conditions $t_r^2 - 4d_r < 0$ or $t_r^2 - 4d_r = 0$ or $t_r^2 - 4d_r > 0$ (see Lemma 4.2 for more descriptions). It follows from classified discussion that we show the main results of this paper in the following six regions:

$$\begin{aligned} \mathcal{G}_{11} &:= \{(t_r, t_l, d_r, d_c, d_l) \in \mathbb{R}^5 \mid t_r > 0, t_l > 0, \\ &\quad d_r > 0, d_c = 0, d_l < 0, t_r^2 - 4d_r < 0\} \subset \mathcal{G}_1, \\ \mathcal{G}_{12} &:= \{(t_r, t_l, d_r, d_c, d_l) \in \mathbb{R}^5 \mid t_r > 0, t_l > 0, \\ &\quad d_r > 0, d_c = 0, d_l < 0, t_r^2 - 4d_r = 0\} \subset \mathcal{G}_1, \\ \mathcal{G}_{13} &:= \{(t_r, t_l, d_r, d_c, d_l) \in \mathbb{R}^5 \mid t_r > 0, t_l > 0, \\ &\quad d_r > 0, d_c = 0, d_l < 0, t_r^2 - 4d_r > 0\} \subset \mathcal{G}_1, \\ \mathcal{G}_{14} &:= \{(t_r, t_l, d_r, d_c, d_l) \in \mathbb{R}^5 \mid t_r > 0, t_l > 0, \\ &\quad d_r > 0, d_c < 0, d_l < 0, t_r^2 - 4d_r < 0\} \subset \mathcal{G}_1, \\ \mathcal{G}_{15} &:= \{(t_r, t_l, d_r, d_c, d_l) \in \mathbb{R}^5 \mid t_r > 0, t_l > 0, \\ &\quad d_r > 0, d_c < 0, d_l < 0, t_r^2 - 4d_r = 0\} \subset \mathcal{G}_1, \\ \mathcal{G}_{16} &:= \{(t_r, t_l, d_r, d_c, d_l) \in \mathbb{R}^5 \mid t_r > 0, t_l > 0, \\ &\quad d_r > 0, d_c < 0, d_l < 0, t_r^2 - 4d_r > 0\} \subset \mathcal{G}_1. \end{aligned}$$

In Theorem 2.1, we give the main results of system (1) as $(t_r, t_l, d_r, d_c, d_l) \in \mathcal{G}_{11}$, i.e., saddle-zero-focus.

Theorem 2.1 For arbitrarily fixed $(t_r, t_l, d_r, d_c, d_l) \in \mathcal{G}_{11}$, the bifurcation diagram of system (1) in the αt_c -plane consists of the following bifurcation curves:

(a) degenerate boundary equilibrium bifurcation curves

$$\begin{aligned} DB_1 &= \{(\alpha, t_c) \in \mathbb{R}^2 \mid \alpha = 0, t_c > 0\}, \\ DB_2 &= \{(\alpha, t_c) \in \mathbb{R}^2 \mid \alpha = 0, t_c < 0\}; \end{aligned}$$

(b) homoclinic bifurcation curve

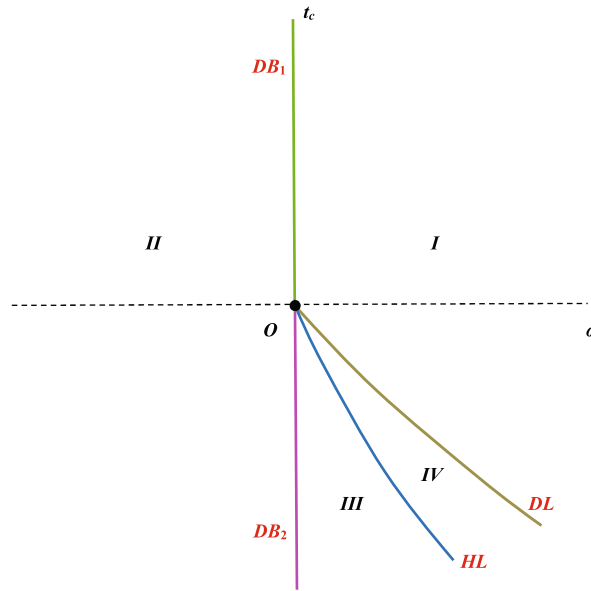
$$HL = \{(\alpha, t_c) \in \mathbb{R}^2 \mid \alpha > 0, t_c = \varphi(\alpha)\};$$

(c) double limit cycle bifurcation curve

$$DL = \{(\alpha, t_c) \in \mathbb{R}^2 \mid \alpha > 0, t_c = \phi(\alpha)\},$$

where the function $t_c = \varphi(\alpha)$ is continuous and monotonous, the function $t_c = \phi(\alpha)$ is continuous, $\varphi(\alpha) < \phi(\alpha) < -t_r(\alpha + \sqrt{4\alpha d_r + \alpha^2})/(2d_r)$ for $\alpha > 0$. Moreover, the bifurcation diagram and global phase portraits in the Poincaré disc of system (1) in \mathcal{G}_{11} can be shown completely in Fig. 1, where

$$\begin{aligned} I &= \{(\alpha, t_c) \in \mathbb{R}^2 \mid \alpha > 0, t_c > \phi(\alpha)\}, \\ II &= \{(\alpha, t_c) \in \mathbb{R}^2 \mid \alpha < 0\}, \\ III &= \{(\alpha, t_c) \in \mathbb{R}^2 \mid \alpha > 0, t_c < \varphi(\alpha)\}, \\ IV &= \{(\alpha, t_c) \in \mathbb{R}^2 \mid \alpha > 0, \varphi(\alpha) < t_c < \phi(\alpha)\}, \\ O &= \{(\alpha, t_c) \in \mathbb{R}^2 \mid \alpha = t_c = 0\}. \end{aligned}$$



(a) The bifurcation diagram in the αt_c -plane of system (1) as $(t_r, t_l, d_r, d_c, d_l) \in \mathcal{G}_{11}$

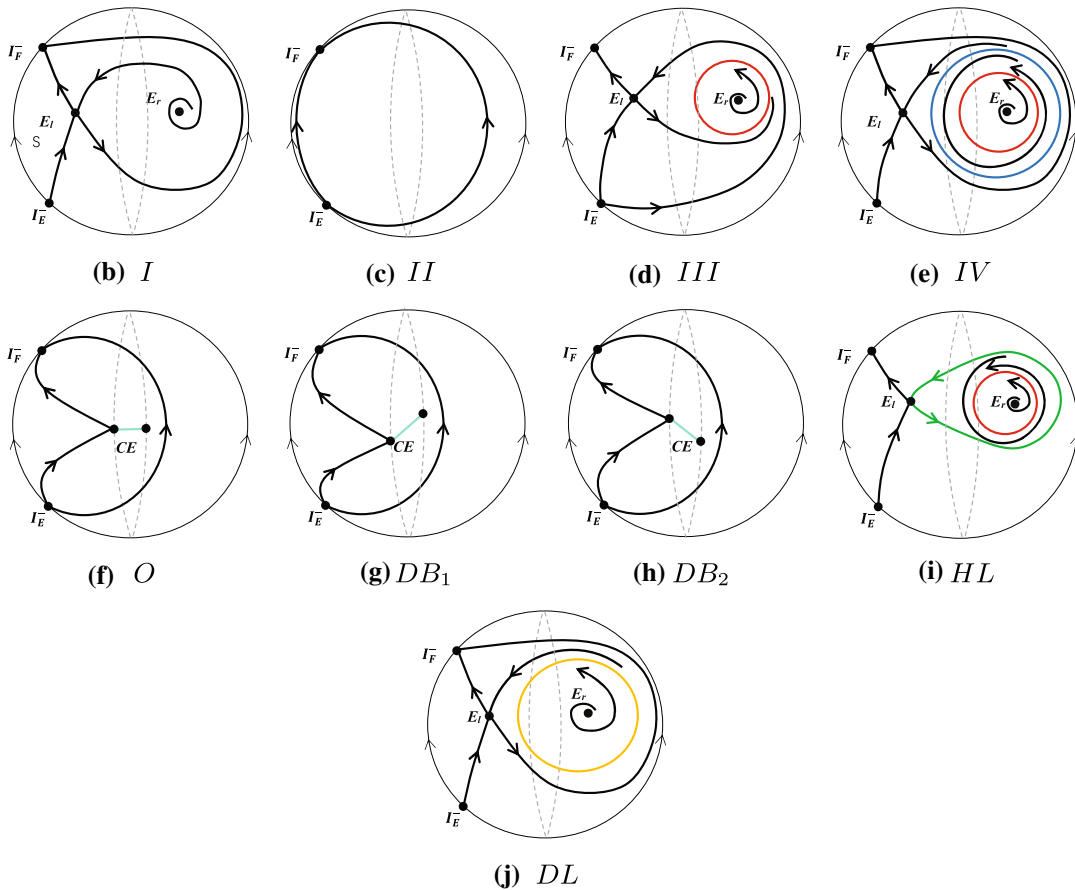


Fig. 1 The bifurcation diagram and global phase portraits in the Poincaré disc of system (1) as $(t_r, t_l, d_r, d_c, d_l) \in \mathcal{G}_{11}$

Remark 1 In Theorem 2.1, it should be noticed that the stable limit cycle is highlighted by red color, the unstable limit cycle is highlighted by blue color, the semi-stable limit cycle is highlighted by yellow color, and the homoclinic loop is highlighted by green color. So is Theorem 2.4. Moreover, in Theorem 2.1, the stable limit cycle involves two or three linear zones, the unstable limit cycle involves three linear zones, the semi-stable limit cycle involves three linear zones, the unstable homoclinic loop involves three linear zones (see Lemmas 5.2 and 5.3 for more descriptions). Besides, the global phase portrait in the Poincaré disc of the region *I* shown in Fig. 1b means that system (1) has two finite equilibrium points E_l and E_r , where E_l is a saddle and E_r is an unstable focus. The stable manifold of E_l in the upper half plane connects the unstable focus E_r and the unstable manifold of E_l in the upper half plane connects the stable manifold of I_F^- . The stable manifold of E_l in the lower half plane connects the unstable manifold of I_E^- and the unstable manifold of E_l in the lower half plane connects the stable manifold of I_F^- . The global phase portrait in the Poincaré disc of the region *II* displayed in Fig. 1c implies that system (1) has neither finite equilibrium points and nor limit cycles. The global phase portrait in the Poincaré disc of the region *III* illustrated in Fig. 1d means that system (1) has two finite equilibrium points E_l and E_r and a unique limit cycle that is stable, where E_l is a saddle and E_r is an unstable focus. The stable manifold of E_l in the upper half plane connects the unstable manifold of I_E^- and the unstable manifold of E_l in the upper half plane connects the stable manifold of I_F^- . The stable manifold of E_l in the lower half plane connects the unstable manifold of I_E^- and the unstable manifold of E_l in the lower half plane approaches the stable limit cycle. And the unstable focus E_r also approaches the stable limit cycle. Due to similarity, we omit the introductions of the remaining global phase portraits in the Poincaré disc of Theorem 2.1 and so are Theorems 2.2, 2.3, 2.4, 2.5 and 2.6.

We give the main results of system (1) as $(t_r, t_l, d_r, d_c, d_l) \in \mathcal{G}_{12}$ in the following theorem, i.e., saddle-zero-improper node.

Theorem 2.2 For arbitrarily fixed $(t_r, t_l, d_r, d_c, d_l) \in \mathcal{G}_{12}$, the bifurcation diagram of system (1) in the αt_c -plane consists of degenerate boundary equilibrium bifurcation curves DB_1 and DB_2 . Moreover, the bifurcation diagram and global phase portraits in the

Poincaré disc of system (1) in \mathcal{G}_{12} can be shown completely in Fig. 2, where

$$\begin{aligned} V &= \{(\alpha, t_c) \in \mathbb{R}^2 \mid \alpha > 0\}, \\ VI &= \{(\alpha, t_c) \in \mathbb{R}^2 \mid \alpha < 0\}, \\ O &= \{(\alpha, t_c) \in \mathbb{R}^2 \mid \alpha = t_c = 0\}. \end{aligned}$$

In Theorem 2.3, we give the main results of system (1) as $(t_r, t_l, d_r, d_c, d_l) \in \mathcal{G}_{13}$, i.e., saddle-zero-bidirectional node.

Theorem 2.3 For arbitrarily fixed $(t_r, t_l, d_r, d_c, d_l) \in \mathcal{G}_{13}$, the bifurcation diagram of system (1) in the αt_c -plane consists of degenerate boundary equilibrium bifurcation curves DB_1 and DB_2 . Moreover, the bifurcation diagram and global phase portraits in the Poincaré disc of system (1) in \mathcal{G}_{13} can be shown completely in Fig. 3, where

$$\begin{aligned} VII &= \{(\alpha, t_c) \in \mathbb{R}^2 \mid \alpha > 0\}, \\ VIII &= \{(\alpha, t_c) \in \mathbb{R}^2 \mid \alpha < 0\}, \\ O &= \{(\alpha, t_c) \in \mathbb{R}^2 \mid \alpha = t_c = 0\}. \end{aligned}$$

We give the main results of system (1) as $(t_r, t_l, d_r, d_c, d_l) \in \mathcal{G}_{14}$ in the following theorem, i.e., saddle–saddle-focus.

Theorem 2.4 For arbitrarily fixed $(t_r, t_l, d_r, d_c, d_l) \in \mathcal{G}_{14}$, the bifurcation diagram of system (1) in the αt_c -plane consists of the following bifurcation curves:

(a) boundary equilibrium bifurcation curves

$$\begin{aligned} BE_1 &= \{(\alpha, t_c) \in \mathbb{R}^2 \mid \alpha = -d_c\}, \\ BE_2 &= \{(\alpha, t_c) \in \mathbb{R}^2 \mid \alpha = d_c\}; \end{aligned}$$

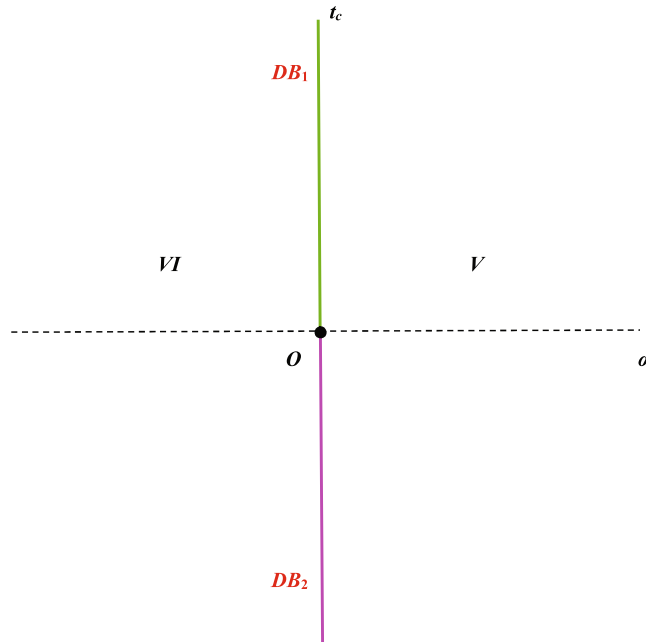
(b) homoclinic bifurcation curves

$$\begin{aligned} HL_2 &= \{(\alpha, t_c) \in \mathbb{R}^2 \mid d_c < \alpha < -d_c, t_c = h(\alpha)\}, \\ HL_3 &= \{(\alpha, t_c) \in \mathbb{R}^2 \mid \alpha > -d_c, t_c = \varphi(\alpha)\}; \end{aligned}$$

(c) double limit cycle bifurcation curve

$$DL_2 = \{(\alpha, t_c) \in \mathbb{R}^2 \mid \alpha > -d_c, t_c = \phi(\alpha)\},$$

where the function $t_c = h(\alpha)$ is continuous satisfying $h(\alpha) < 0$, the function $t_c = \varphi(\alpha)$ is continuous and monotonous and the function $t_c = \phi(\alpha)$ is continuous satisfying $\varphi(\alpha) < \phi(\alpha) < -t_r(\alpha - d_c + \sqrt{4\alpha d_r + (\alpha - d_c)^2})/(2d_r)$ for $\alpha > -d_c$. Moreover, the bifurcation diagram and global phase portraits in



(a) The bifurcation diagram in the αt_c -plane of system (1) as $(t_r, t_l, d_r, d_c, d_l) \in \mathcal{G}_{12}$

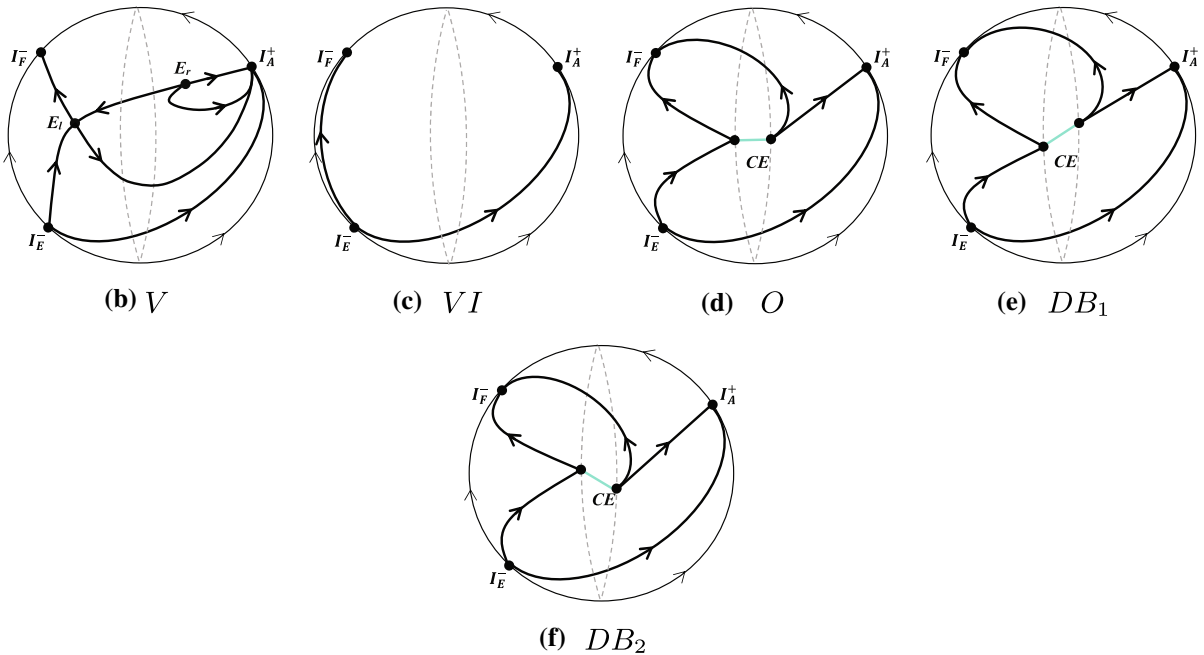
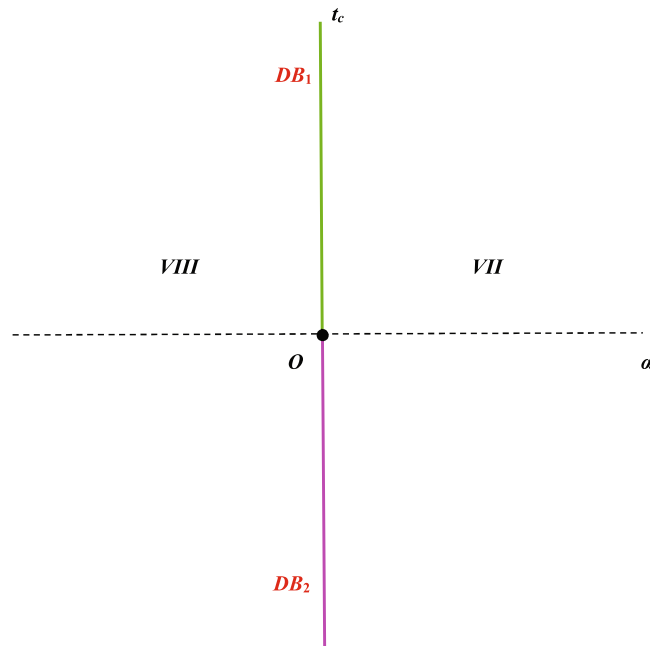


Fig. 2 The bifurcation diagram and global phase portraits in the Poincaré disc of system (1) as $(t_r, t_l, d_r, d_c, d_l) \in \mathcal{G}_{12}$



(a) The bifurcation diagram in the αt_c -plane of system (1) as $(t_r, t_l, d_r, d_c, d_l) \in \mathcal{G}_{13}$

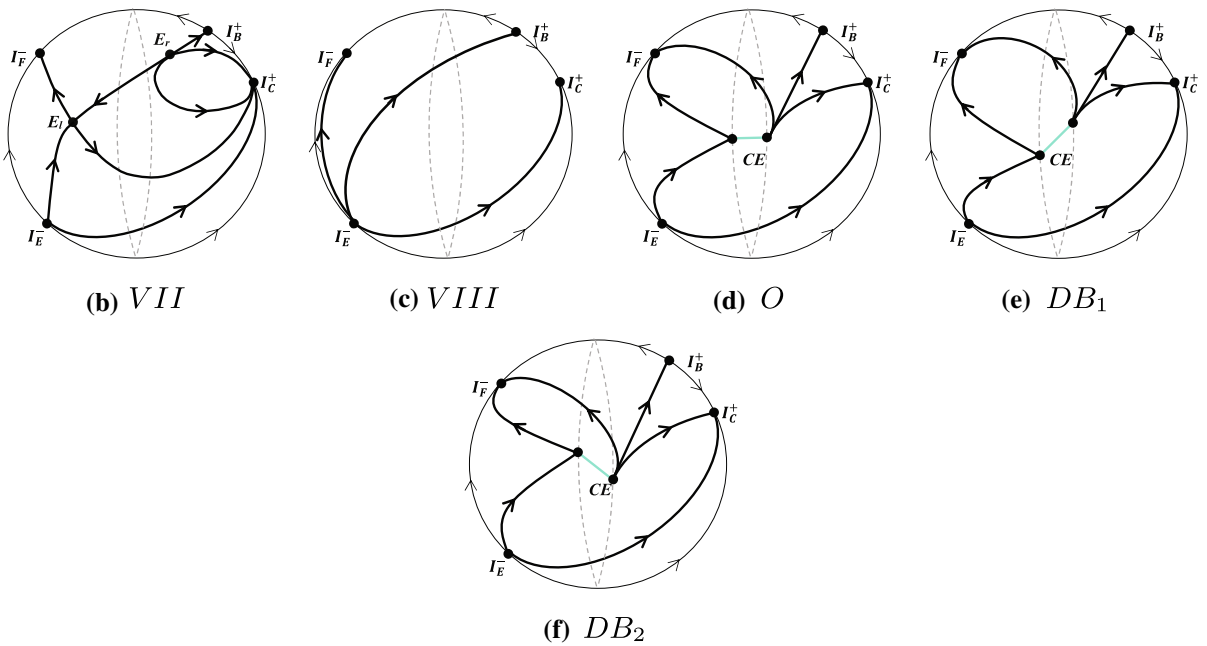


Fig. 3 The bifurcation diagram and global phase portraits in the Poincaré disc of system (1) as $(t_r, t_l, d_r, d_c, d_l) \in \mathcal{G}_{13}$

the Poincaré disc of system (1) in \mathcal{G}_{14} can be shown completely in Fig. 4, where

$$\begin{aligned} R_1 &= \{(\alpha, t_c) \in \mathbb{R}^2 \mid \alpha > -d_c, t_c > \phi(\alpha)\}, \\ R_2 &= \{(\alpha, t_c) \in \mathbb{R}^2 \mid d_c < \alpha < -d_c, t_c > h(\alpha)\}, \\ R_3 &= \{(\alpha, t_c) \in \mathbb{R}^2 \mid \alpha < d_c\}, \\ R_4 &= \{(\alpha, t_c) \in \mathbb{R}^2 \mid d_c < \alpha < -d_c, t_c < h(\alpha)\}, \\ R_5 &= \{(\alpha, t_c) \in \mathbb{R}^2 \mid \alpha > -d_c, t_c < \varphi(\alpha)\}, \\ R_6 &= \{(\alpha, t_c) \in \mathbb{R}^2 \mid \alpha > -d_c, \varphi(\alpha) < t_c < \phi(\alpha)\}, \\ BE_{11} &= \{(\alpha, t_c) \in \mathbb{R}^2 \mid \alpha = -d_c, t_c > h(\alpha)\}, \\ BE_{12} &= \{(\alpha, t_c) \in \mathbb{R}^2 \mid \alpha = -d_c, t_c = h(\alpha)\}, \\ BE_{13} &= \{(\alpha, t_c) \in \mathbb{R}^2 \mid \alpha = -d_c, t_c < h(\alpha)\}. \end{aligned}$$

Remark 2 In Theorem 2.4, the stable limit cycle involves two or three linear zones when $\alpha > -d_c$ and involves two linear zones when $d_c < \alpha \leq -d_c$, the unstable limit cycle involves three linear zones, the semi-stable limit cycle involves three linear zones, and the homoclinic loop involves three linear zones (see Lemmas 5.2, 5.3 and 5.6 for more descriptions). Moreover, the homoclinic loop is unstable when $\alpha > -d_c$ and is stable when $d_c < \alpha \leq -d_c$. Notice that global phase portraits in the Poincaré disc of $HL_3, DL_2, R_1, R_3, R_5$ and R_6 of Theorem 2.4 are the same with global phase portraits in the Poincaré disc of HL, DL, I, II, III and IV of Theorem 2.1, respectively.

In Theorem 2.5, we give the main results of system (1) as $(t_r, t_l, d_r, d_c, d_l) \in \mathcal{G}_{15}$, i.e., saddle–saddle-improper node.

Theorem 2.5 For arbitrarily fixed $(t_r, t_l, d_r, d_c, d_l) \in \mathcal{G}_{15}$, the bifurcation diagram of system (1) in the αt_c -plane consists of boundary equilibrium bifurcation curves BE_1 and BE_2 . Moreover, the bifurcation diagram and global phase portraits in the Poincaré disc of system (1) in \mathcal{G}_{15} can be shown completely in Fig. 5, where

$$\begin{aligned} R_7 &= \{(\alpha, t_c) \in \mathbb{R}^2 \mid \alpha > -d_c\}, \\ R_8 &= \{(\alpha, t_c) \in \mathbb{R}^2 \mid d_c < \alpha < -d_c\}, \\ R_9 &= \{(\alpha, t_c) \in \mathbb{R}^2 \mid \alpha < d_c\}. \end{aligned}$$

Remark 3 Note that global phase portraits in the Poincaré disc of R_7 and R_9 of Theorem 2.5 are the

same with global phase portraits in the Poincaré disc of V and VI of Theorem 2.2, respectively.

We give the main results of system (1) as $(t_r, t_l, d_r, d_c, d_l) \in \mathcal{G}_{16}$ in the following theorem, i.e., saddle–saddle-bidirectional node.

Theorem 2.6 For arbitrarily fixed $(t_r, t_l, d_r, d_c, d_l) \in \mathcal{G}_{16}$, the bifurcation diagram of system (1) in the αt_c -plane consists of boundary equilibrium bifurcation curves BE_1 and BE_2 . Moreover, the bifurcation diagram and global phase portraits in the Poincaré disc of system (1) in \mathcal{G}_{16} can be shown completely in Fig. 6, where

$$\begin{aligned} R_{10} &= \{(\alpha, t_c) \in \mathbb{R}^2 \mid \alpha > -d_c\}, \\ R_{11} &= \{(\alpha, t_c) \in \mathbb{R}^2 \mid d_c < \alpha < -d_c\}, \\ R_{12} &= \{(\alpha, t_c) \in \mathbb{R}^2 \mid \alpha < d_c\}. \end{aligned}$$

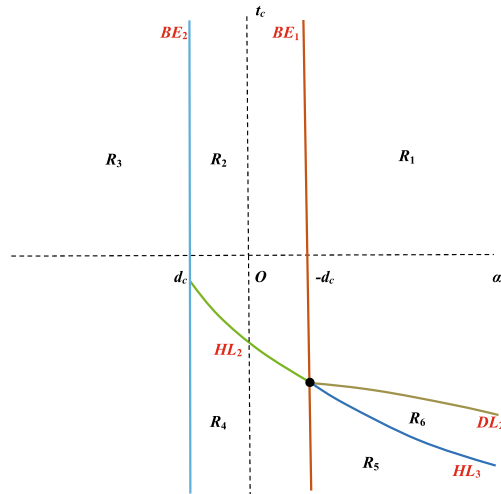
Remark 4 Notice that global phase portraits in the Poincaré disc of R_{10} and R_{12} of Theorem 2.6 are the same with global phase portraits in the Poincaré disc of VII and $VIII$ of Theorem 2.3, respectively.

3 Application to a second-order memristor oscillator

Memristor is a two-terminal circuit element, for which a nonlinear relationship links charge and flux, presented by Chua [16]. For the realization of memristor, see [2, 38, 40] and references therein. In 2011, Corinto et al. gave a mathematical model for a second-order memristor oscillator in [17]. Here, we use our main results in Sect. 2 to analyze a second-order memristor oscillator with a flux-controlled memristor, see Fig. 7 or [17].

Firstly, we recall the mathematical model of a second-order memristor oscillator with a flux-controlled memristor. In this circuit, the values of L and C for the impedance and capacitance are positive constants, while the resistor R has a negative value. Two Kirchhoff’s Current Law linearly independent equations and two Kirchhoff’s Voltage Law linearly independent equations for this circuit are as follows

$$\begin{aligned} i_R(t) - i_L(t) &= 0, \\ i_L(t) - i_C(t) - i_M(t) &= 0, \\ v_R(t) + v_L(t) + v_C(t) &= 0, \\ v_C(t) - v_M(t) &= 0, \end{aligned} \tag{2}$$



(a) The bifurcation diagram in the αt_c -plane of system (1) as $(t_r, t_l, d_r, d_c, d_l) \in \mathcal{G}_{14}$

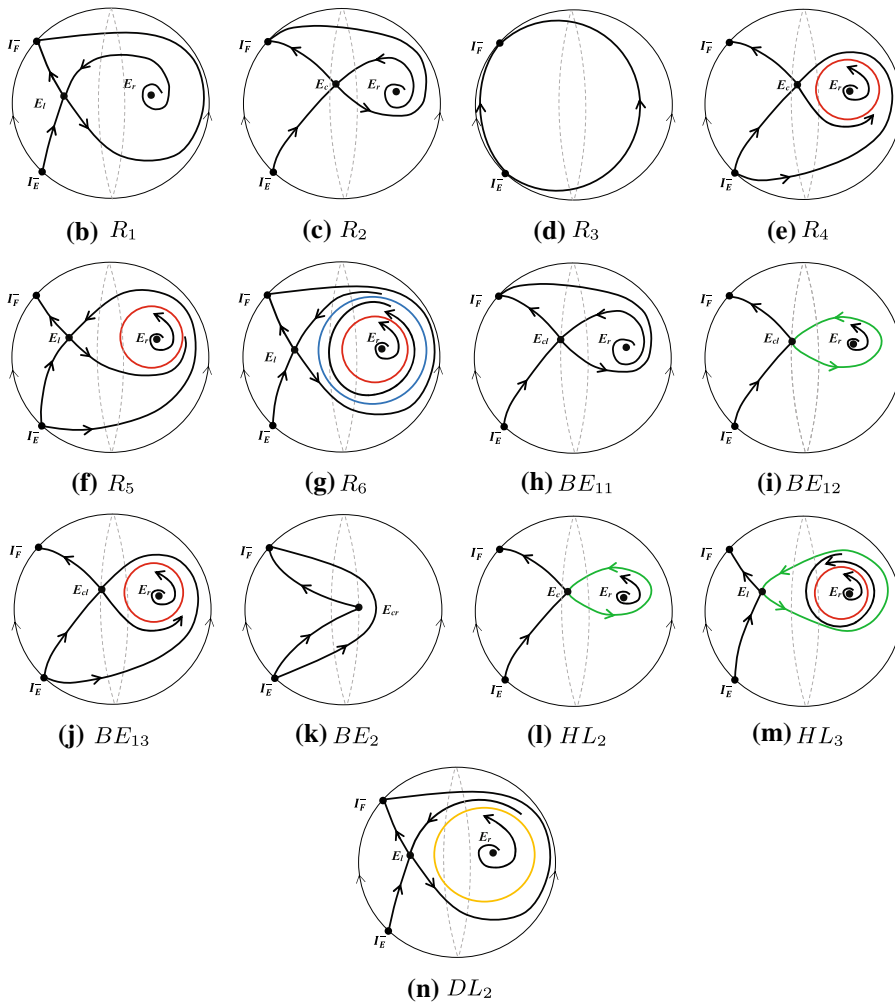
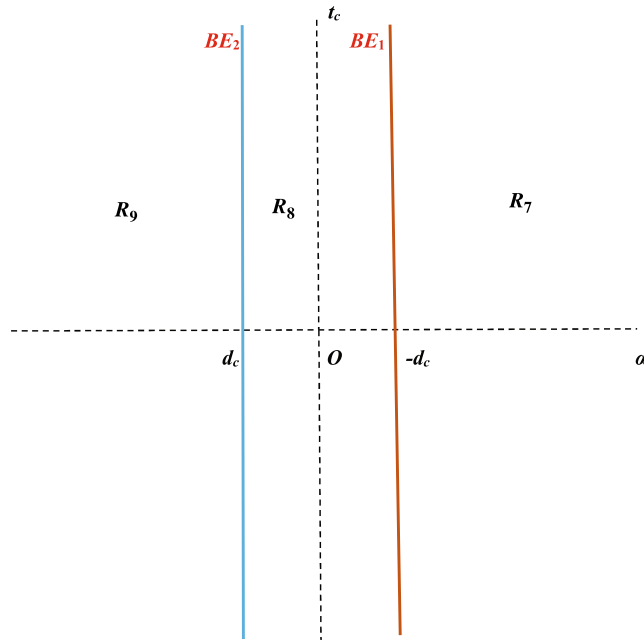


Fig. 4 The bifurcation diagram and global phase portraits in the Poincaré disc of system (1) as $(t_r, t_l, d_r, d_c, d_l) \in \mathcal{G}_{14}$



(a) The bifurcation diagram in the αt_c -plane of system (1) as $(t_r, t_l, d_r, d_c, d_l) \in \mathcal{G}_{15}$

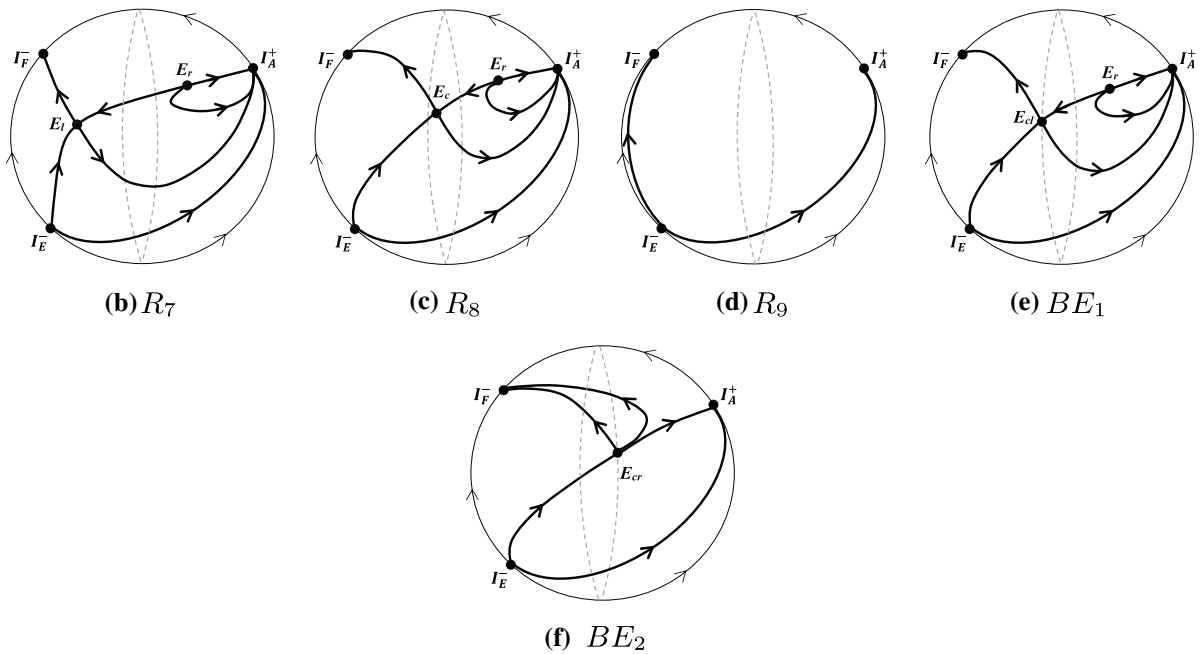
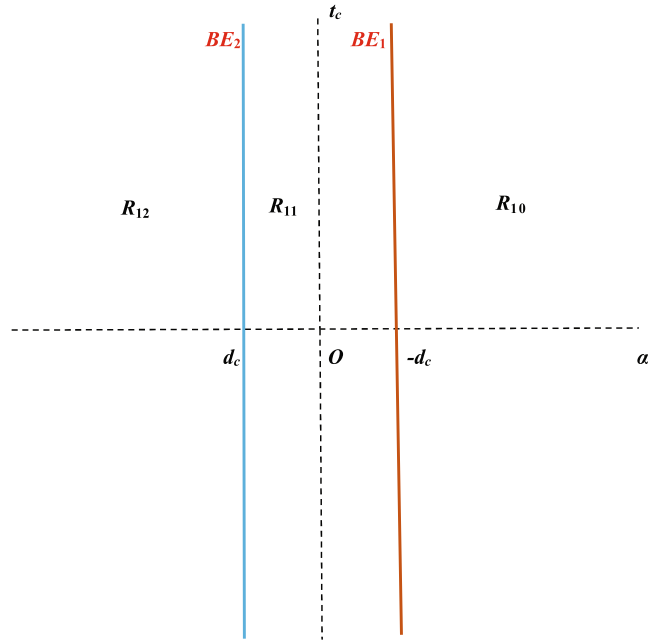


Fig. 5 The bifurcation diagram and global phase portraits in the Poincaré disc of system (1) as $(t_r, t_l, d_r, d_c, d_l) \in \mathcal{G}_{15}$



(a) The bifurcation diagram in the αt_c -plane of system (1) as $(t_r, t_l, d_r, d_c, d_l) \in \mathcal{G}_{16}$

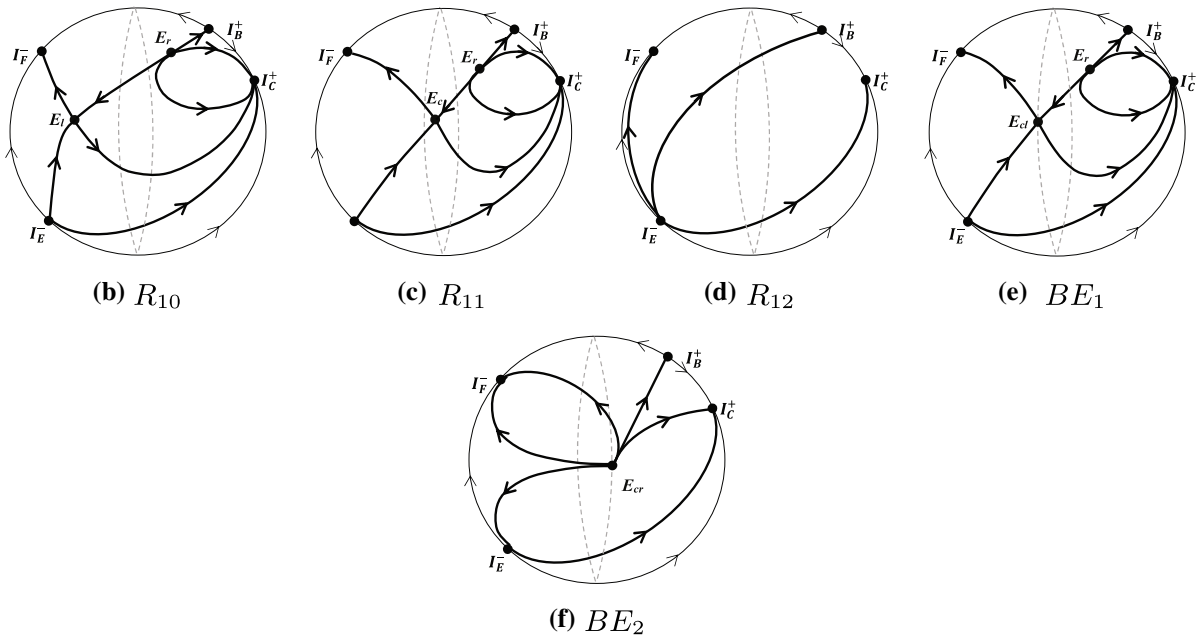


Fig. 6 The bifurcation diagram and global phase portraits in the Poincaré disc of system (1) as $(t_r, t_l, d_r, d_c, d_l) \in \mathcal{G}_{16}$

where i and v denote current and voltage of the corresponding element of this circuit, respectively. Integrating both sides of each equation in (2) from time instant t_0 to time instant t , we obtain

$$\begin{aligned} q_R(t) - q_L(t) &= Q_1, \\ q_L(t) - q_C(t) - q_M(t) &= Q_2, \\ \varphi_R(t) + \varphi_L(t) + \varphi_C(t) &= \Phi_1, \\ \varphi_C(t) - \varphi_M(t) &= \Phi_2, \end{aligned} \tag{3}$$

where q and φ represent charge and flux of the corresponding element of this circuit, respectively, and let $Q_1 = Q_2 = \Phi_1 = \Phi_2 = 0$ as explained in Section II of [17]. Besides, the constitutive equations of the involved bipoles for this circuit are as follows

$$\begin{aligned} q_M(t) &= q_m(\varphi_M(t)), \\ q_C(t) &= C \frac{d}{dt} \varphi_C(t), \\ \varphi_R(t) &= Rq_R(t), \\ \varphi_L(t) &= L \frac{d}{dt} q_L(t), \end{aligned} \tag{4}$$

where q_m stand for the flux-charge characteristic of the memristor. It follows from (3) and (4) that we get

$$\begin{aligned} \frac{d}{dt} \varphi_C(t) &= \frac{q_C(t)}{C} = \frac{1}{C}[q_L(t) - q_M(t)] \\ &= \frac{1}{C}[q_L(t) - q_m(\varphi_C(t))], \\ \frac{d}{dt} q_L(t) &= \frac{\varphi_L(t)}{L} = \frac{1}{L}[-\varphi_R(t) - \varphi_C(t)] \\ &= \frac{1}{L}[-Rq_L(t) - \varphi_C(t)]. \end{aligned}$$

Denote $x := \varphi_C(t)$ and $y := q_L(t)$. Then, we have

$$\frac{dx}{dt} = \frac{1}{C}[-q_m(x) + y], \quad \frac{dy}{dt} = \frac{1}{L}[-x - Ry], \tag{5}$$

where $q_m(x)$ may be described by the following Lur'e model (see [17])

$$L(D)x(t) = -q_m(x(t)),$$

and

$$L(D) = \frac{D^2 + \frac{R}{L}D + \frac{1}{CL}}{\frac{1}{C}(D + \frac{R}{L})} = \frac{CLD^2 + CRD + 1}{LD + R}.$$

Instead of the symmetric piecewise linear function

$$q_m(x) = \begin{cases} b(x - 1) + a, & \text{if } x > 1, \\ ax, & \text{if } -1 \leq x \leq 1, \\ b(x + 1) - a, & \text{if } x < -1 \end{cases}$$

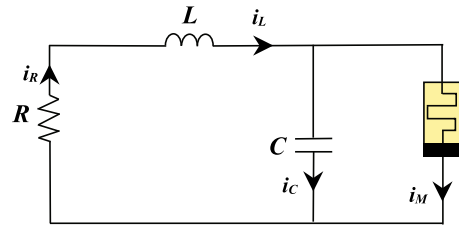


Fig. 7 A second-order memristor oscillator with a flux-controlled memristor

considered in [17,24], we adopt here a more general model for the nonlinear flux-charge characteristic of the memristor, namely

$$q_m(x) = \begin{cases} a_1(x - v) + a_2v, & \text{if } x > v, \\ a_2x, & \text{if } -u \leq x \leq v, \\ a_3(x + u) - a_2u, & \text{if } x < -u, \end{cases} \tag{6}$$

where v and u are positive constants.

Secondly, we change system (5) with (6) into system (1). We first use the time scaling transformation $t \rightarrow C\tau$ to change system (5) into

$$\frac{dx}{d\tau} = -q_m(x) + y, \quad \frac{dy}{d\tau} = -\frac{C}{L}[x + Ry]. \tag{7}$$

Second, under the linear transformation $\tilde{x} \rightarrow x, \tilde{y} \rightarrow -y - RCx/L$, system (7) can be written as

$$\begin{aligned} \frac{d\tilde{x}}{d\tau} &= -q_m(\tilde{x}) - \frac{RC}{L}\tilde{x} - \tilde{y} := F_m(\tilde{x}) - \tilde{y}, \\ \frac{d\tilde{y}}{d\tau} &= \frac{RC}{L}q_m(\tilde{x}) + \frac{C}{L}\tilde{x} := g(\tilde{x}), \end{aligned} \tag{8}$$

where

$$\begin{aligned} F_m(\tilde{x}) &= \begin{cases} b_1(\tilde{x} - v) + b_2v, & \text{if } \tilde{x} > v, \\ b_2\tilde{x}, & \text{if } -u \leq \tilde{x} \leq v, \\ b_3(\tilde{x} + u) - b_2u, & \text{if } \tilde{x} < -u, \end{cases} \\ g_m(\tilde{x}) &= \begin{cases} b_4(\tilde{x} - v) + b_5v, & \text{if } \tilde{x} > v, \\ b_5\tilde{x}, & \text{if } -u \leq \tilde{x} \leq v, \\ b_6(\tilde{x} + u) - b_5u, & \text{if } \tilde{x} < -u, \end{cases} \end{aligned}$$

and

$$\begin{aligned} b_1 &= -a_1 - \frac{RC}{L}, \\ b_2 &= -a_2 - \frac{RC}{L}, \\ b_3 &= -a_3 - \frac{RC}{L}, \end{aligned}$$

$$\begin{aligned}
 b_4 &= \frac{RC}{L}a_1 + \frac{C}{L}, \\
 b_5 &= \frac{RC}{L}a_2 + \frac{C}{L}, \\
 b_6 &= \frac{RC}{L}a_3 + \frac{C}{L}.
 \end{aligned}$$

Third, with the translation transformation $\tilde{x} \rightarrow \bar{x} + (-u + v)/2$, $\tilde{y} \rightarrow \bar{y} + b_2(-u + v)/2$, system (8) becomes

$$\frac{d\bar{x}}{d\tau} = \overline{F_m}(\bar{x}) - \bar{y}, \quad \frac{d\bar{y}}{d\tau} = \overline{g_m}(\bar{x}), \tag{9}$$

where

$$\begin{aligned}
 \overline{F_m}(x) &= \begin{cases} b_1(\bar{x} - \frac{u+v}{2}) + \frac{b_2(u+v)}{2}, & \text{if } \bar{x} > \frac{u+v}{2}, \\ b_2\bar{x}, & \text{if } -\frac{u+v}{2} \leq \bar{x} \leq \frac{u+v}{2}, \\ b_3(\bar{x} + \frac{u+v}{2}) - \frac{b_2(u+v)}{2}, & \text{if } \bar{x} < -\frac{u+v}{2}, \end{cases} \\
 \overline{g_m}(x) &= \begin{cases} b_4(\bar{x} - \frac{u+v}{2}) + b_5v, & \text{if } \bar{x} > \frac{u+v}{2}, \\ b_5\bar{x} + \frac{b_5(-u+v)}{2}, & \text{if } -\frac{u+v}{2} \leq \bar{x} \leq \frac{u+v}{2}, \\ b_6(\bar{x} + \frac{u+v}{2}) - b_5u, & \text{if } \bar{x} < -\frac{u+v}{2}. \end{cases}
 \end{aligned}$$

Finally, by the scaling transformation $\bar{x} \rightarrow (u + v)x/2$, $\bar{y} \rightarrow (u + v)y/2$, $\tau \rightarrow t$, system (9) can be written as system (1) with

$$t_r = b_1, \quad t_c = b_2, \quad t_l = b_3,$$

and

$$d_r = b_4, \quad d_c = b_5, \quad d_l = b_6, \quad \alpha = b_5 \frac{u - v}{u + v}.$$

We are now able to apply our main results in Sect. 2 in a convenient way, and we do not attempt to address all statements, but only the most important cases. Consider the case of a non-symmetric second-order memristor oscillator with three linear zones in the situation corresponding to $t_r > 0, t_l > 0, d_r > 0, d_l < 0$, which is not considered in [17, 24]. The conditions $t_r > 0, t_l > 0, d_r > 0, d_l < 0$ mean that $a_1 \in (-\infty, -1/R), a_3 \in (-1/R, -RC/L)$ when $R^2C > L$ holds. If $a_2 = -1/R$ in system (5), we have $d_c = \alpha = 0$ in system (1). A direct application of Theorem 2.1 gives the following result.

Proposition 3.1 *Consider a second-order memristor oscillator with a flux-controlled memristor, as modeled by system (5) with (6). Under the design condition $R^2C > L$, if the additional hypotheses $a_1 \in (-\infty, -1/R), a_2 = -1/R, a_3 \in (-1/R, -RC/L)$ are fulfilled, then the circuit exhibits no limit cycles.*

If $a_2 > -1/R$ of system (5), we have $d_c < 0$ and $-d_c < \alpha < d_c$ in system (1). A direct application of Theorem 2.4 gives the following result.

Proposition 3.2 *Consider a second-order memristor oscillator with a flux-controlled memristor, as modeled by system (5) with (6). Under the design condition $R^2C > L$, if the additional hypotheses $a_1 \in (-\infty, -1/R), a_2 \in (-1/R, +\infty), a_3 \in (-1/R, -RC/L)$ are fulfilled, then the circuit exhibits a stable limit cycle if and only if $a_2 \in (-RC/L - h(\alpha), +\infty)$, where $\alpha := (RCa_2/L + C/L)(u - v)/(u + v)$ and $h(\alpha) < 0$ is a continuous function on $t_c := -a_2 - RC/L$.*

4 Local dynamics of system (1)

4.1 Finite equilibrium point

Lemma 4.1 *When $d_c \leq 0$ in \mathcal{G}_1 , system (1) exhibits no equilibrium point if $\alpha < d_c$; one continuum of non-isolated equilibrium points CE (resp. one isolated equilibrium point E_{cr}) if $\alpha = d_c = 0$ (resp. $\alpha = d_c < 0$); two isolated equilibrium points E_c and E_r if $d_c < \alpha < -d_c$ and $d_c < 0$; two isolated equilibrium points E_{cl} and E_r if $\alpha = -d_c > 0$; and two isolated equilibrium points E_l and E_r if $\alpha > -d_c$. The qualitative properties of these equilibrium points are shown in Table 1, where $E_{cl} : (-1, -t_c)$ lies on the left switching line Γ_l ; $E_{cr} : (1, t_c)$ lies on the right switching line Γ_r ; $E_l : ((\alpha + d_c)/d_l - 1, t_l(\alpha + d_c)/d_l - t_c)$ lies in S_l ; $E_c : (\alpha/d_c, t_c\alpha/d_c)$ lies in S_c ; $E_r : ((\alpha - d_c)/d_r + 1, t_r(\alpha - d_c)/d_r + t_c)$ lies in S_r ; and $CE : \{(x, y) \in \mathbb{R}^2 \mid y = t_c x, -1 \leq x \leq 1\}$ lies in $\Gamma_l \cup S_c \cup \Gamma_r$.*

Proof Solving $\dot{x} = \dot{y} = 0$ for system (1), the number of equilibrium points of system (1) is determined by the relationship between α and d_c , as shown in Table 1. Notice that the Jacobian matrices at E_l, E_c and E_r have, respectively, the following forms

$$\begin{aligned}
 J_{E_l} &:= \begin{bmatrix} t_l & -1 \\ d_l & 0 \end{bmatrix}, \quad J_{E_c} := \begin{bmatrix} t_c & -1 \\ d_c & 0 \end{bmatrix}, \\
 J_{E_r} &:= \begin{bmatrix} t_r & -1 \\ d_r & 0 \end{bmatrix}.
 \end{aligned}$$

Then, we have $\text{tr} J_{E_l} = t_l, \text{tr} J_{E_c} = t_c, \text{tr} J_{E_r} = t_r, \det J_{E_l} = d_l, \det J_{E_c} = d_c$ and $\det J_{E_r} = d_r$. Hence, we

Table 1 The qualitative properties of finite equilibrium point of system (1) with $d_c \leq 0$ in \mathcal{G}_1

Possibilities $t_r, t_c, d_r, d_c, \alpha$				Number, stability and type	
$d_c = 0$	$\alpha < 0$			0	
	$\alpha = 0$	$t_c < 0$	$t_r^2 - 4d_r < 0$	1, CE generalized cusp (see Fig. 9a)	
			$t_r^2 - 4d_r = 0$	1, CE generalized saddle-nodde (see Fig. 9b)	
			$t_r^2 - 4d_r > 0$	1, CE generalized saddle-nodde (see Fig. 9c)	
	$t_c = 0$	$t_c = 0$	$t_r^2 - 4d_r < 0$	1, CE generalized cusp (see Fig. 9d)	
			$t_r^2 - 4d_r = 0$	1, CE generalized saddle-nodde (see Fig. 9e)	
			$t_r^2 - 4d_r > 0$	1, CE generalized saddle-nodde (see Fig. 9f)	
	$t_c > 0$	$t_c > 0$	$t_r^2 - 4d_r < 0$	1, CE generalized cusp (see Fig. 9g)	
			$t_r^2 - 4d_r = 0$	1, CE generalized saddle-nodde (see Fig. 9h)	
			$t_r^2 - 4d_r > 0$	1, CE generalized saddle-nodde (see Fig. 9i)	
	$d_c < 0$	$\alpha > 0$			
		$\alpha < d_c$	$\alpha < d_c$	$t_r^2 - 4d_r < 0$	2, E_l saddle, E_r unstable focus
$t_r^2 - 4d_r = 0$				2, E_l saddle, E_r unstable node	
$t_r^2 - 4d_r > 0$				0	
$\alpha = d_c$		$\alpha = d_c$	$t_r^2 - 4d_r < 0$	1, E_{cr} cusp (see Fig. 8a)	
			$t_r^2 - 4d_r = 0$	1, E_{cr} saddle-node (see Fig. 8b)	
			$t_r^2 - 4d_r > 0$	1, E_{cr} saddle-node (see Fig. 8c)	
$d_c < \alpha < -d_c$		$d_c < \alpha < -d_c$	$t_r^2 - 4d_r < 0$	2, E_c saddle, E_r unstable focus	
			$t_r^2 - 4d_r \geq 0$	2, E_c saddle, E_r unstable node	
			$t_r^2 - 4d_r < 0$	2, E_{cl} saddle, E_r unstable focus	
$\alpha = -d_c$		$\alpha = -d_c$	$t_r^2 - 4d_r < 0$	2, E_{cl} saddle, E_r unstable focus	
			$t_r^2 - 4d_r \geq 0$	2, E_{cl} saddle, E_r unstable node	
	$t_r^2 - 4d_r < 0$		2, E_l saddle, E_r unstable focus		
$\alpha > -d_c$	$\alpha > -d_c$	$t_r^2 - 4d_r < 0$	2, E_l saddle, E_r unstable focus		
		$t_r^2 - 4d_r \geq 0$	2, E_l saddle, E_r unstable node		

can easily obtain the topological type and stability of E_l, E_c and E_r , as indicated in Table 1.

We secondly study the equilibrium points of system (1) that lie on the switching line $x = 1$ or $x = -1$ when $d_c < 0$. The equilibrium point E_{cr} , as seen from \mathcal{S}_c is a saddle, but when seen from \mathcal{S}_r is a focus (resp. node) for $t_r^2 - 4d_r < 0$ (resp. ≥ 0). According to the fact that solutions of system (1) satisfy the existence, uniqueness and continuity with respect to initial conditions and parameters, it follows that the qualitative property of E_{cr} is a cusp (resp. saddle-node) for $t_r^2 - 4d_r < 0$ (resp. ≥ 0), as displayed in Fig. 8a (resp. b–c). The equilibrium point E_{cl} as seen from both \mathcal{S}_l and \mathcal{S}_c is a saddle, it follows that E_{cl} is a saddle.

We finally investigate the continuum of non-isolated equilibrium points CE . Note that the left endpoint of segment CE in \mathcal{S}_l is a half of a saddle and the right endpoint of segment CE in \mathcal{S}_r is a half of a focus (resp. improper node; bidirectional node) for $t_r^2 - 4d_r < 0$ (resp. $= 0; > 0$). All orbits and the singular contin-

uum $y = 0$ are parallel to each other in the region $\{(x, y) \in \mathbb{R}^2 | -1 \leq x \leq 1\}$ when $t_c = 0$. It follows that the qualitative property of CE is illustrated in Fig. 9d–f when $t_c = 0$. When $t_c \neq 0$, all orbits which lie above $y = t_c x$ with $|x| \leq 1$ are the negative horizontal direction and those orbits which lie under $y = t_c x$ with $|x| \leq 1$ are the positive horizontal direction. Therefore, the qualitative property of CE is displayed in Fig. 9a–c, g–i when $t_c < 0$ and $t_c > 0$, respectively. The proof of Lemma 4.1 is complete. \square

4.2 Equilibrium point at infinity

We investigate the qualitative property of equilibrium point at infinity, which reflects the tendencies of x or y in a large domain. Despite system (1) is not a polynomial dynamical system, we can still study the equilibrium point at infinity with the Poincaré transformation (for the validity of the Poincaré transformation, one can

Fig. 8 The qualitative property of E_{cr} of system (1) with $\alpha = d_c < 0$ in \mathcal{G}_1

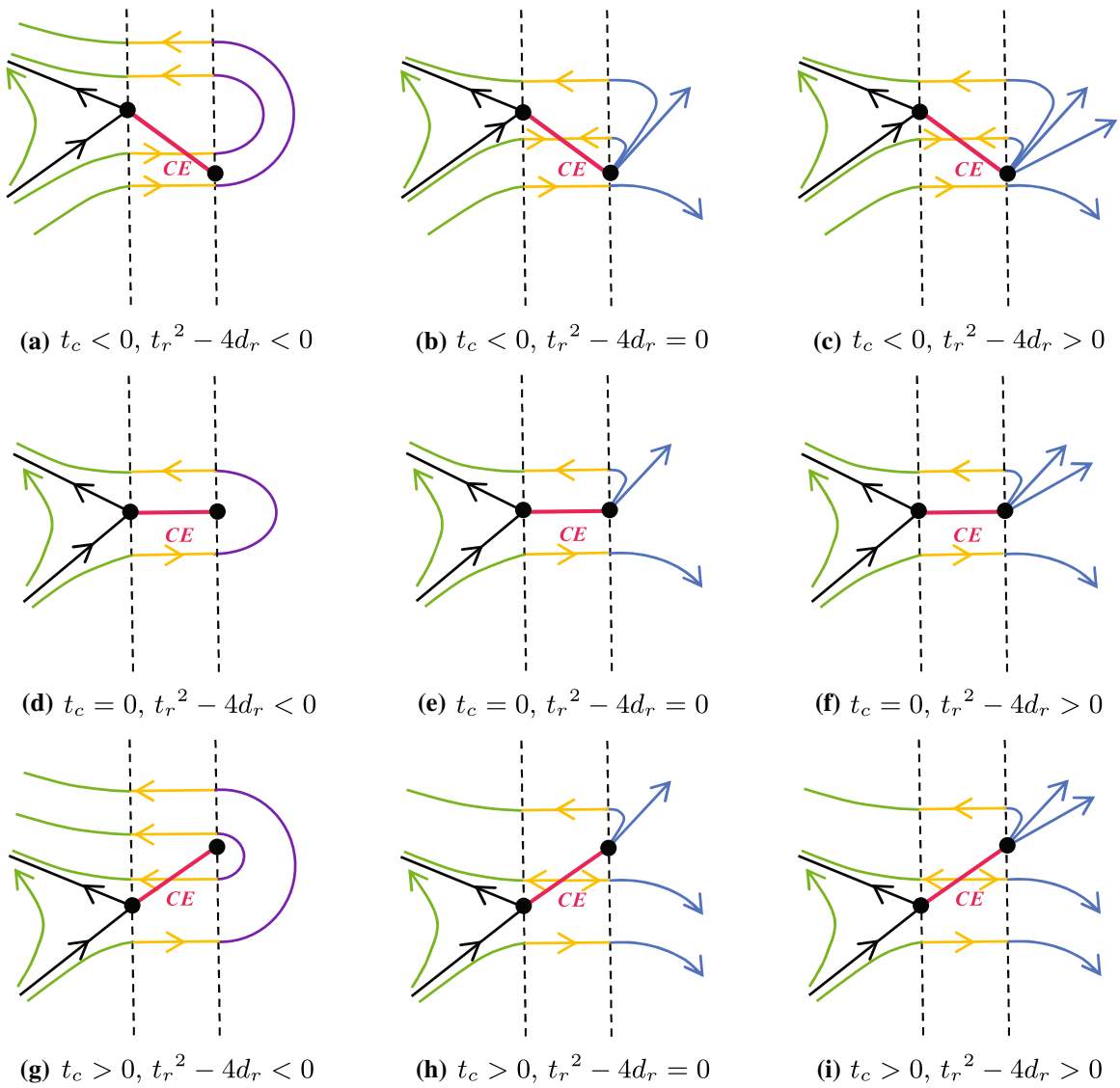
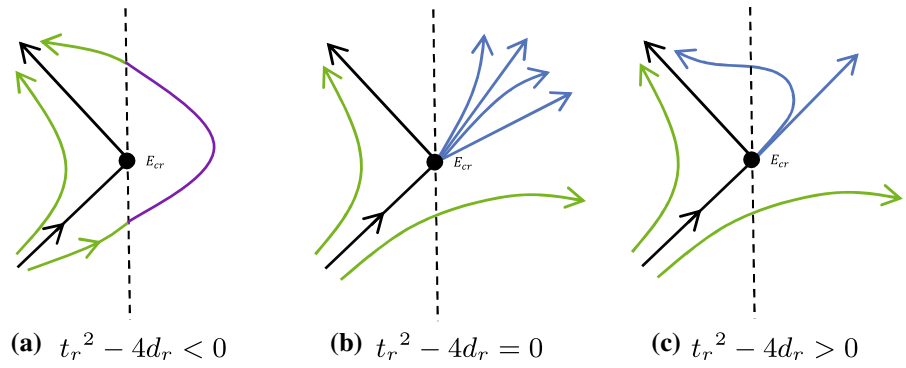
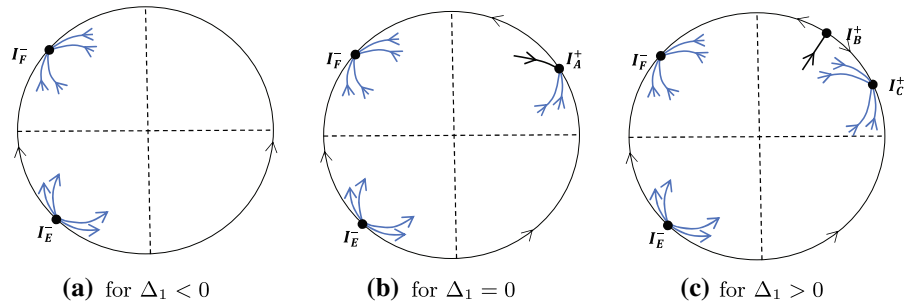


Fig. 9 The qualitative property of CE of system (1) with $\alpha = d_c = 0$ in \mathcal{G}_1

Fig. 10 The equilibrium points at infinity in the Poincaré disc of system (1) in \mathcal{G}_1



refer to the Poincaré compactification in Chapter 2.9 of [29]).

Lemma 4.2 *The equilibrium points at infinity in the Poincaré disc of system (1) are shown in Fig. 10 when parameters belong to the region \mathcal{G}_1 , where $\Delta_1 := t_r^2 - 4d_r$.*

Proof With a Poincaré transformation $x = 1/z$, $y = u/z$, system (1) is changed into

$$\begin{aligned} \frac{du}{dt} &= \frac{d_r + d_l}{2} - \frac{t_r + t_l}{2}u + \left(\frac{d_l - d_r}{2} - \alpha\right)z \\ &\quad - \frac{t_l - t_r}{2}uz + u^2 - \frac{t_c - t_l}{2}u|1 + z|\operatorname{sgnz} \\ &\quad - \frac{t_r - t_c}{2}u|1 - z|\operatorname{sgnz} + \frac{d_c - d_l}{2}|1 + z|\operatorname{sgnz} \\ &\quad + \frac{d_r - d_c}{2}|1 - z|\operatorname{sgnz}, \\ \frac{dz}{dt} &= -\frac{t_r + t_l}{2}z - \frac{t_l - t_r}{2}z^2 \\ &\quad + uz - \frac{t_c - t_l}{2}|1 + z||z| - \frac{t_r - t_c}{2}|1 - z||z|. \end{aligned} \tag{10}$$

Since we only need to investigate the qualitative property of equilibrium point of system (10) that lies on the u -axis, we write system (10) as

$$\begin{aligned} \frac{du}{dt} &= \frac{d_r + d_l}{2} + \frac{d_r - d_l}{2}\operatorname{sgnz} \\ &\quad - \frac{t_r + t_l}{2}u + \frac{t_l - t_r}{2}u\operatorname{sgnz} \\ &\quad + \left(\frac{d_l - d_r}{2} - \alpha\right)z + \frac{2d_c - d_r - d_l}{2}|z| \\ &\quad - \frac{t_l - t_r}{2}uz + u^2 + \left(\frac{t_r + t_l - 2t_c}{2}\right)u|z|, \\ \frac{dz}{dt} &= -\frac{t_r + t_l}{2}z - \frac{t_l - t_r}{2}z^2 + uz \end{aligned}$$

$$+ \frac{t_l - t_r}{2}|z| + \frac{t_r + t_l - 2t_c}{2}z|z|, \tag{11}$$

by $|1 + z| = 1 + z$ and $|1 - z| = 1 - z$ as $z \rightarrow 0$. When $z \rightarrow 0^+$ and $z \rightarrow 0^-$, system (11) becomes

$$\begin{aligned} \frac{du}{dt} &= d_r - t_r u + u^2 + (-d_r + d_c - \alpha)z + (t_r - t_c)uz, \\ \frac{dz}{dt} &= -t_r z + uz + (t_r - t_c)z^2, \end{aligned} \tag{12}$$

and

$$\begin{aligned} \frac{du}{dt} &= d_l - t_l u + u^2 + (d_l - d_c - \alpha)z + (-t_l + t_c)uz, \\ \frac{dz}{dt} &= -t_l z + uz + (-t_l + t_c)z^2, \end{aligned} \tag{13}$$

respectively. According to the fact that solutions of system (1) satisfy the existence, uniqueness and continuity with respect to initial conditions and parameters, we turn to investigate the qualitative property of equilibrium point of systems (12) and (13) that lies on the u -axis to obtain the qualitative property of equilibrium point of system (11) that lies on the u -axis.

Consider system (12). Notice that the number of equilibrium point of system (12) depends on the roots of the equation

$$u^2 - t_r u + d_r = 0.$$

Therefore, system (12) has no equilibrium point when $\Delta_1 < 0$, a unique equilibrium point $A : (t_r/2, 0)$ when $\Delta_1 = 0$, two equilibrium points $B : ((t_r + \sqrt{\Delta_1})/2, 0)$ and $C : ((t_r - \sqrt{\Delta_1})/2, 0)$ when $\Delta_1 > 0$. Clearly, A , B and C all lie on the positive u -axis. Let I_A^+ , I_B^+ and I_C^+ be the corresponding equilibrium point at infinity of A , B and C in the xy -plane, respectively. Then, I_A^+ , I_B^+ and I_C^+ in the first quadrant in the Poincaré disc because of $z \rightarrow 0^+$.

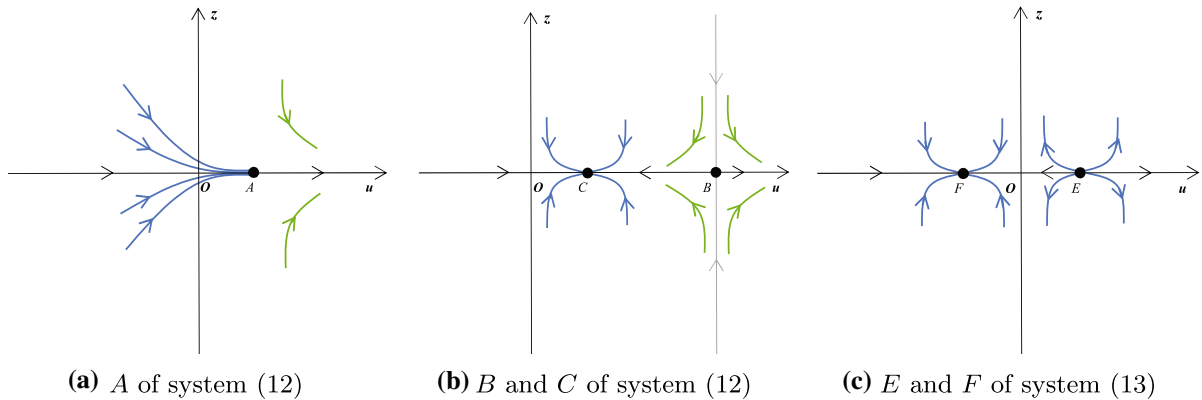


Fig. 11 The qualitative property of A, B, C, E and F

Consider system (13). We define

$$\Delta_2 := (-t_l)^2 - 4d_l.$$

It is obvious that $\Delta_2 > 0$. It follows from the equation

$$u^2 - t_l u + d_l = 0$$

that system (13) has two equilibrium points $E : ((t_l + \sqrt{\Delta_2})/2, 0)$ and $F : ((t_l - \sqrt{\Delta_2})/2, 0)$. Evidently, E and F lie on the positive and negative u -axis, respectively. Set I_E^- and I_F^- be the corresponding equilibrium point at infinity of E and F in the xy -plane, respectively. Due to $z \rightarrow 0^-$, I_E^- and I_F^- lie in the third quadrant and the second quadrant in the Poincaré disc, respectively.

We now study the qualitative property of A, B, C, E and F in turn. First, consider A . For simplicity, we change system (12) into

$$\begin{aligned} \frac{du}{dt} &= (d_c + d_r - \alpha - t_r t_c / 2)z + (t_r - t_c)uz + u^2, \\ \frac{dz}{dt} &= -t_r z / 2 + uz + (t_r - t_c)z^2, \end{aligned} \tag{14}$$

by the translation transformation $u \rightarrow u + t_r / 2, z \rightarrow z$. It means that A is moved to the origin of system (14). Note that the Jacobian matrix at the origin of system (14) has a non-zero eigenvalue and a zero eigenvalue. Solving $(d_c + d_r - \alpha - t_r t_c / 2)z + (t_r - t_c)uz + u^2 = 0$, we obtain

$$z = \frac{2}{t_r t_c + 2(\alpha - d_r - d_c)} u^2 + O(u^3) \tag{15}$$

by the implicit function theorem. Substituting (15) into the second equation of system (14), we get

$$\frac{dz}{dt} = -\frac{t_r}{t_r t_c + 2(\alpha - d_r - d_c)} u^2 + O(u^3).$$

According to Theorem 7.1 of [41, Chapter 2], the origin of system (14) is a saddle-node and so is A , as shown in Fig. 11a.

Second, consider B . By the translation transformation $u \rightarrow u + (t_r + \sqrt{\Delta_1})/2, z \rightarrow z$, system (12) becomes

$$\begin{aligned} \frac{du}{dt} &= \sqrt{\Delta_1} u + [-d_r + d_c - \alpha \\ &\quad + (t_r - t_c)(t_r + \sqrt{\Delta_1})/2]z + (t_r - t_c)uz + u^2, \\ \frac{dz}{dt} &= (-t_r + \sqrt{\Delta_1})z/2 + uz + (t_r - t_c)z^2, \end{aligned} \tag{16}$$

which implies that B is moved to the origin of system (16). The Jacobian matrix at the origin of system (16) has the following form

$$J_1 := \begin{bmatrix} \sqrt{\Delta_1} - d_r + d_c - \alpha + (t_r - t_c)(t_r + \sqrt{\Delta_1})/2 & \\ 0 & (-t_r + \sqrt{\Delta_1})/2 \end{bmatrix}.$$

Due to $\det J_1 = \sqrt{\Delta_1}(-t_r + \sqrt{\Delta_1})/2 < 0$, the origin of system (16) is a saddle. So is B , as shown in Fig. 11b.

Third, consider C . In order to move C to the origin, we can rewrite system (12) as

$$\begin{aligned} \frac{du}{dt} &= -\sqrt{\Delta_1} u + [-d_r + d_c - \alpha \\ &\quad + (t_r - t_c)(t_r - \sqrt{\Delta_1})/2]z + (t_r - t_c)uz + u^2, \\ \frac{dz}{dt} &= (-t_r - \sqrt{\Delta_1})z/2 + uz + (t_r - t_c)z^2, \end{aligned} \tag{17}$$

by the translation transformation $u \rightarrow u + (t_r - \sqrt{\Delta_1})/2, z \rightarrow z$. It is simple to obtain the Jacobian matrix at the origin of system (17) as follows

$$J_2 := \begin{bmatrix} -\sqrt{\Delta_1} - d_r + d_c - \alpha + (t_r - t_c)(t_r - \sqrt{\Delta_1})/2 & \\ 0 & (-t_r - \sqrt{\Delta_1})/2 \end{bmatrix}.$$

Evidently, $\text{tr} J_2 = -\sqrt{\Delta_1} + (-t_r - \sqrt{\Delta_1})/2 < 0$, $\det J_2 = -\sqrt{\Delta_1}(-t_r - \sqrt{\Delta_1})/2 > 0$, $(\text{tr} J_2)^2 - 4\det J_2 > 0$. Thus, the origin of system (17) is a stable node. So is C , as shown in Fig. 11b.

Then, consider E . With the translation transformation $u \rightarrow u + (t_l + \sqrt{\Delta_2})/2, z \rightarrow z$, system (13) can be changed into

$$\begin{aligned} \frac{du}{dt} &= \sqrt{\Delta_2}u + [d_l - d_c - \alpha \\ &\quad + (-t_l + t_c)(t_l + \sqrt{\Delta_2})/2]z + (-t_l + t_c)uz + u^2, \\ \frac{dz}{dt} &= (-t_l + \sqrt{\Delta_2})z/2 + uz + (-t_l + t_c)z^2. \end{aligned} \quad (18)$$

It means that E is moved to the origin of system (18). We easily have the Jacobian matrix at the origin of system (18) as follows

$$J_3 := \begin{bmatrix} \sqrt{\Delta_2} d_l - d_c - \alpha + (-t_l + t_c)(t_l + \sqrt{\Delta_2})/2 & \\ 0 & (-t_l + \sqrt{\Delta_2})/2 \end{bmatrix}.$$

It follows from $\text{tr} J_3 = \sqrt{\Delta_2} + (-t_l + \sqrt{\Delta_2})/2 > 0$, $\det J_3 = \sqrt{\Delta_2}(-t_l + \sqrt{\Delta_2})/2 > 0$ and $(\text{tr} J_3)^2 - 4\det J_3 > 0$ that the origin of system (18) is an unstable node. So is E , as shown in Fig. 11c.

Finally, consider F . We can change system (13) into

$$\begin{aligned} \frac{du}{dt} &= -\sqrt{\Delta_2}u + [d_l - d_c - \alpha \\ &\quad + (-t_l + t_c)(t_l - \sqrt{\Delta_2})/2]z + (-t_l + t_c)uz + u^2, \\ \frac{dz}{dt} &= (-t_l - \sqrt{\Delta_2})z/2 + uz + (-t_l + t_c)z^2, \end{aligned} \quad (19)$$

by the translation transformation $u \rightarrow u + (t_l - \sqrt{\Delta_2})/2, z \rightarrow z$. It implies that F is moved to the origin of system (19). Obviously, the Jacobian matrix at the origin of system (19) has the following form

$$J_4 := \begin{bmatrix} -\sqrt{\Delta_2} d_l - d_c - \alpha + (-t_l + t_c)(t_l - \sqrt{\Delta_2})/2 & \\ 0 & (-t_l - \sqrt{\Delta_2})/2 \end{bmatrix}.$$

Since $\text{tr} J_4 = -\sqrt{\Delta_2} + (-t_l - \sqrt{\Delta_2})/2 < 0$, $\det J_4 = -\sqrt{\Delta_2}(-t_l - \sqrt{\Delta_2})/2 > 0$ and $(\text{tr} J_4)^2 - 4\det J_4 > 0$, the origin of system (19) is a stable node. So is F , as shown in Fig. 11c.

In order to analyze equilibrium point at infinity on the y -axis, we use another Poincaré transformation $x = v/z, y = 1/z$ to change system (1) into the form

$$\begin{aligned} \frac{dv}{dt} &= -1 + \frac{t_r + t_l}{2}v + \frac{t_l - t_r}{2}z \\ &\quad + \left(\alpha - \frac{d_l - d_r}{2}\right)vz - \frac{d_r + d_l}{2}v^2 \\ &\quad + \frac{t_c - t_l}{2}|v + z|\text{sgnz} \\ &\quad + \frac{t_r - t_c}{2}|v - z|\text{sgnz} - \frac{d_c - d_l}{2}|v + z|v\text{sgnz} \\ &\quad - \frac{d_r - d_c}{2}|v - z|v\text{sgnz}, \\ \frac{dz}{dt} &= \left(\alpha - \frac{d_l - d_r}{2}\right)z^2 - \frac{d_r + d_l}{2}vz \\ &\quad - \frac{d_c - d_l}{2}|v + z||z| - \frac{d_r - d_c}{2}|v - z||z|. \end{aligned} \quad (20)$$

It is obvious that $(0, 0)$ is not an equilibrium point of system (20). It means that the corresponding points at infinity of system (1) on the y -axis are not equilibrium point at infinity. By the aforementioned analysis, we obtain the equilibrium point at infinity of system (1) in the Poincaré disc, as shown in Fig. 10. This completes the proof. \square

5 Nonlocal dynamics of system (1)

In this section, we study limit cycles and homoclinic loops of system (1) in the case $d_c \leq 0$ when parameters belong to the region \mathcal{G}_1 . From Lemma 4.1, we know that system (1) has no equilibrium point for $\alpha < d_c \leq 0$, a unique continuum of non-isolated equilibrium point CE for $\alpha = d_c = 0$, a unique equilibrium point E_{cr} for $\alpha = d_c < 0$, two equilibrium points for $\alpha > d_c$ and $d_c \leq 0$. It follows from Lemma 4.1 that CE lies in $\Gamma_l \cup \mathcal{S}_c \cup \Gamma_r$ and is a half of a saddle in \mathcal{S}_l , which means that system (1) has two invariant lines in \mathcal{S}_l . Then it implies that there is no limit cycle surrounding CE . By Lemma 4.1 again, we obtain that E_{cr} lies on the right switching line Γ_r and is a half of a node in \mathcal{S}_r for $t_r^2 - 4d_r \geq 0$, which implies that system (1) has at least one invariant line in \mathcal{S}_r . Then it means that there is no limit cycle surrounding E_{cr} as $t_r^2 - 4d_r \geq 0$. When $t_r^2 - 4d_r < 0$, assume that there exists limit cycle surrounding E_{cr} . Then, any limit cycles must intersect with $y = y_{E_{cr}}$, where $y_{E_{cr}}$ represents the ordinate of

E_{cr} . However, we have $\dot{y}|_{y=y_{E_{cr}}} > 0$. This is a contradiction implying that there is no limit cycle surrounding E_{cr} as $t_r^2 - 4d_r < 0$.

By the aforementioned discussion, we only need to study limit cycles and homoclinic loops of system (1) with $d_c \leq 0$ and $\alpha > d_c$ in \mathcal{G}_1 .

In what follows, consider $d_c \leq 0$ and $\alpha > d_c$ in \mathcal{G}_1 . Denote

$$e := \frac{\alpha - d_c}{d_r}.$$

Evidently, $e > 0$ because of $\alpha > d_c$ and $d_r > 0$. Then, the coordinate of E_r of system (1) can represent as $(e + 1, t_r e + t_c)$. Using the translation transformation $x \rightarrow x + e + 1, \quad y \rightarrow y + t_r e + t_c,$

system (1) is changed into

$$\frac{dx}{dt} = \widehat{F}(x) - y, \quad \frac{dy}{dt} = \widehat{g}(x), \tag{21}$$

where

$$\widehat{F}(x) = \begin{cases} t_r x, & \text{if } x > -e, \\ t_c x + (t_c - t_r)e, & \text{if } -e - 2 \leq x \leq -e, \\ t_l(x + e + 2) - t_r e - 2t_c, & \text{if } x < -e - 2, \end{cases}$$

and

$$\widehat{g}(x) = \begin{cases} d_r x, & \text{if } x > -e, \\ d_c x + (d_c - d_r)e, & \text{if } -e - 2 \leq x \leq -e, \\ d_l(x + e + 2) - d_r e - 2d_c, & \text{if } x < -e - 2, \end{cases}$$

which means that E_r of system (1) is moved to $O : (0, 0)$ of system (21), while E_c of system (1) is moved to $N_c : ((d_r/d_c - 1)e, (t_c d_r/d_c - t_r)e)$ of system (21) if $d_c < \alpha < -d_c$ and $d_c < 0$; E_{cl} of system (1) is moved to $N_{cl} : (-e - 2, -t_r e - 2t_c)$ of system (21) if $\alpha = -d_c$ and $d_c < 0$; E_l of system (1) is moved to $N_l : ((d_r/d_l - 1)e + 2d_c/d_l - 2, (t_l d_r/d_l - t_r)e - 2t_c + 2t_l d_c/d_l)$ of system (21) if $\alpha > -d_c$ and $d_c \leq 0$.

The plane \mathbb{R}^2 can be divided into three open linear zones

$$\mathcal{S}_{\widehat{\Gamma}} = \{(x, y) \in \mathbb{R}^2 | x < -e - 2\},$$

$$\mathcal{S}_{\widehat{c}} = \{(x, y) \in \mathbb{R}^2 | -e - 2 < x < -e\},$$

$$\mathcal{S}_{\widehat{r}} = \{(x, y) \in \mathbb{R}^2 | x > -e\}$$

by two straight lines $\Gamma_{\widehat{\Gamma}} = \{(x, y) \in \mathbb{R}^2 | x = -e - 2\}$ and $\Gamma_{\widehat{r}} = \{(x, y) \in \mathbb{R}^2 | x = -e\}$. For notations simplicity, for system (21) we still use F and g to represent \widehat{F} and \widehat{g} , respectively.

Since system (21) is topologically equivalent to system (1), it suffices to study limit cycles and homoclinic loops of system (21) to obtain the corresponding results

of system (1) by a translation transformation. System (21) exhibits two equilibrium points O and N_l when $d_c \leq 0$ and $\alpha > -d_c$ or O and N_{cl} (resp. N_c) when $d_c < 0$ and $\alpha = -d_c$ (resp. $d_c < \alpha < -d_c$). Applying Lemma 4.1, we obtain that N_l, N_{cl} and N_c are saddles; O is an unstable node for $t_r^2 - 4d_r \geq 0$ or an unstable focus for $t_r^2 - 4d_r < 0$. By [41, Chapter 4], we know that the index of a saddle is -1 , the index of a node is 1, the index of a focus is 1, and the sum of the indices of all equilibrium points surrounded by a limit cycle is 1. Therefore, limit cycles of system (21) must only surround O if it exists. According to the location of saddle point of system (21), we divide our study into two subcases $d_c \leq 0, \alpha > -d_c$ and $d_c < 0, d_c < \alpha \leq -d_c$.

5.1 Limit cycles and homoclinic loops of system (1) with $d_c \leq 0$ and $\alpha > -d_c$ in \mathcal{G}_1

We first give the nonexistence of limit cycles and homoclinic loops of system (1) in the following lemma, when $d_c \leq 0$ and $\alpha > -d_c$ in \mathcal{G}_1 .

Lemma 5.1 *When $d_c \leq 0, \alpha > -d_c$ in \mathcal{G}_1 , system (1) exhibits neither limit cycles nor homoclinic loops, if one of the following statements holds:*

- (a) $t_r^2 - 4d_r \geq 0$;
- (b) $t_r^2 - 4d_r < 0$ and $t_c \geq t_c^*$, where $t_c^* := \frac{-t_r(\alpha - d_c + \sqrt{4\alpha d_r + (\alpha - d_c)^2})}{2d_r}$.

Proof Consider $t_r^2 - 4d_r \geq 0$. Then, N_l of system (21) is a saddle and O of system (21) is an unstable node. System (21) has at least one invariant line in $\mathcal{S}_{\widehat{r}}$ implying that any orbit passing the switching line $\Gamma_{\widehat{r}}$ has no intersections with the switching line $\Gamma_{\widehat{\Gamma}}$ again. Hence, system (21) exhibits neither limit cycles nor homoclinic loops. So is system (1).

Consider $t_r^2 - 4d_r < 0$. Then, N_l of system (21) is a saddle and O of system (21) is an unstable focus. In order to prove the nonexistence of limit cycles and homoclinic loops of system (21), we set a generalized Filippov transformation

$$z(x) := \int_0^x g(s)ds,$$

and $x_1(z)$ and $x_2(z)$ be the branches of the inverse of $z(x)$ for $x \geq 0$ and $x_{N_l} < x < 0$, respectively, where $x_{N_l} := (d_r/d_l - 1)e + 2d_c/d_l - 2$. By system (21), we can calculate that

$$z(x) = \begin{cases} \frac{d_r x^2}{2}, & \text{if } x > -e, \\ \frac{d_c}{2}(x + e)^2 - d_r e x - \frac{d_r}{2} e^2, & \text{if } -e - 2 \leq x \leq -e, \\ \frac{d_l}{2}(x + e + 2)^2 - (d_r e + 2d_c)x - \frac{d_r}{2} e^2 - 2d_c - 2d_c e, & \text{if } x_{N_l} < x < -e - 2. \end{cases} \tag{22}$$

Then

$$z(x) \in \begin{cases} [0, +\infty), & \text{if } x \geq 0, \\ (0, \frac{d_r e^2}{2}), & \text{if } -e < x < 0, \\ [\frac{d_r e^2}{2}, 2d_c + 2d_r e + \frac{d_r e^2}{2}], & \text{if } -e - 2 \leq x \leq -e, \\ (2d_c + 2d_r e + \frac{d_r e^2}{2}, z_{N_l}), & \text{if } x_{N_l} < x < -e - 2, \end{cases}$$

where $z_{N_l} := 2d_c + 2d_r e + d_r e^2/2 - (d_r e + 2d_c)^2/(2d_l)$. It follows from (22) that

$$x_1(z) = \sqrt{\frac{2z}{d_r}}, \quad \text{if } x \geq 0, \tag{23}$$

and

$$x_2(z) = \begin{cases} -\sqrt{\frac{2z}{d_r}}, & \text{if } -e < x < 0, \\ \frac{(d_r - d_c)e - \sqrt{d_r^2 e^2 - d_r d_c e^2 + 2d_c z}}{d_c}, & \text{if } -e - 2 \leq x \leq -e. \end{cases} \tag{24}$$

Define $F_1(z) := F(x_1(z))$ and $F_2(z) := F(x_2(z))$. Our purpose is to prove $F_1(z) > F_2(z)$ for $z \in (0, z_{N_l})$ implying that there are no limit cycles and homoclinic loops, see [32, Section 6]. Based on (23) and (24), we derive

$$F_1(z) = t_r \sqrt{\frac{2z}{d_r}}, \quad \text{if } z > 0, \tag{25}$$

and

$$F_2(z) = \begin{cases} -t_r \sqrt{\frac{2z}{d_r}}, & \text{if } 0 < z < \frac{d_r e^2}{2}, \\ t_c \frac{d_r e - \sqrt{d_r^2 e^2 - d_r d_c e^2 + 2d_c z}}{d_c} - t_r e, & \text{if } \frac{d_r e^2}{2} \leq z \leq 2d_c + 2d_r e + \frac{d_r e^2}{2}. \end{cases} \tag{26}$$

Further, by (25) and (26), we have

$$F_1(z) - F_2(z) = \begin{cases} 2t_r \sqrt{\frac{2z}{d_r}}, & \text{if } 0 < z < \frac{d_r e^2}{2}, \\ t_r \sqrt{\frac{2z}{d_r}} - t_c \frac{d_r e - \sqrt{d_r^2 e^2 - d_r d_c e^2 + 2d_c z}}{d_c} + t_r e, & \text{if } \frac{d_r e^2}{2} \leq z \leq 2d_c + 2d_r e + \frac{d_r e^2}{2}. \end{cases}$$

Evidently, $F_1(z) - F_2(z) > 0$ when $z \in (0, d_r e^2/2)$. For $z \in [d_r e^2/2, 2d_c + 2d_r e + d_r e^2/2]$, a routine computation gives rise to

$$F_1'(z) - F_2'(z) = \frac{t_r \sqrt{d_r^2 e^2 - d_r d_c e^2 + 2d_c z} + t_c \sqrt{2d_r z}}{\sqrt{d_r^2 e^2 - d_r d_c e^2 + 2d_c z} \cdot \sqrt{2d_r z}} > 0$$

when $t_c > 0$ and

$$F_1'(z) - F_2'(z) = \frac{t_r \sqrt{d_r^2 e^2 - d_r d_c e^2 + 2d_c z} + t_c \sqrt{2d_r z}}{\sqrt{d_r^2 e^2 - d_r d_c e^2 + 2d_c z} \cdot \sqrt{2d_r z}} > 0 \text{ (resp. } = 0; < 0),$$

if $z < z_0$ (resp. $z = z_0; z > z_0$),

when $t_c < 0$, where $z_0 := t_r^2(d_r d_c e^2 - d_r^2 e^2)/(2(t_r^2 d_c - t_c^2 d_r))$. For $z \in (2d_c + 2d_r e + d_r e^2/2, z_{N_l})$, by the monotonicity of $F_1(z)$ and $F_2(z)$, we have

$$F_1(z) > F_1(2d_c + 2d_r e + d_r e^2/2),$$

$$F_2(2d_c + 2d_r e + d_r e^2/2) > F_2(z).$$

By the aforementioned discussion, when $z \in (0, z_{N_l})$, it is clear that $F_1(z) - F_2(z) > 0$ is equivalent to

$$(F_1(z) - F_2(z))|_{z=2d_c+2d_r e+\frac{d_r e^2}{2}} = t_r \sqrt{\frac{4d_c + 4d_r e + d_r e^2}{d_r}} + 2t_c + t_r e > 0. \tag{27}$$

Solving (27), we have $t_c > t_c^*$. According to [32, Section 6], it follows that system (21) exhibits neither

limit cycles nor homoclinic loops when $t_c \geq t_c^*$. So is system (1). This completes the proof of Lemma 5.1. \square

Based on Lemma 5.1, we only need to consider the existence of limit cycles of system (1) when $d_c \leq 0$, $\alpha > -d_c$, $t_r^2 - 4d_r < 0$ and $t_c < t_c^*$ in \mathcal{G}_1 .

Lemma 5.2 *Considering $d_c \leq 0$, $\alpha > -d_c$, $t_r^2 - 4d_r < 0$ and $t_c < t_c^*$ in \mathcal{G}_1 , system (1) exhibits at most two limit cycles.*

Proof When $d_c \leq 0$, $\alpha > -d_c$, $t_r^2 - 4d_r < 0$ and $t_c < t_c^*$ in \mathcal{G}_1 , system (21) has two equilibrium points O and N_l , where O is a unstable focus and N_l is a saddle. Since limit cycles of system (21) only surround O by the index theory of [41, Chapter 4] and O lies in $\mathcal{S}_{\widehat{r}}$, it follows that limit cycles of system (21) can be small limit cycle involving two linear zones ($\mathcal{S}_{\widehat{c}}$ and $\mathcal{S}_{\widehat{r}}$) or large limit cycle involving three linear zones if it exists. The existence and uniqueness of small limit cycles of system (21) have proved in [31, Theorem 2] or [12, Theorem 2.2]. Therefore, we can arrive at the conclusion that system (1) has at most one small limit cycle when $d_c \leq 0$, $\alpha > -d_c$, $t_r^2 - 4d_r < 0$ and $t_c < t_c^*$ in \mathcal{G}_1 . Moreover, the small limit cycle is stable if it exists.

It remains to study the number, stability and hyperbolicity of large limit cycles of system (21). Take any two large limit cycles of system (21) denoted as Γ_1 and Γ_2 , where Γ_1 and Γ_2 are adjacent to each other, Γ_1 is the inner most one, $A_i, B_i, C_i, D_i, E_i, F_i, G_i$ and H_i are points on Γ_i , the abscissa of D_i and H_i is $-e$ and the abscissa of E_i and G_i is $-e - 2$ for $i = 1, 2$, as shown in Fig. 12a. Our purpose is to prove

$$\oint_{\Gamma_2} F'(x)dt > \oint_{\Gamma_1} F'(x)dt. \tag{28}$$

Let $y_1(x)$ and $y_2(x)$ represent the orbit segments $\widehat{C_1E_1}$ and $\widehat{C_2E_2}$, respectively. Therefore,

$$\begin{aligned} & \int_{\widehat{C_1E_1}} F'(x)dt \\ &= \int_0^{-e-2} \frac{F'(x)}{F(x) - y_1(x)} dx \\ &= \int_0^{-e-2} \frac{(F'(x) - y_1'(x)) + y_1'(x)}{F(x) - y_1(x)} dx \\ &= \int_0^{-e-2} \frac{1}{F(x) - y_1(x)} d(F(x) - y_1(x)) \\ & \quad + \int_0^{-e-2} \frac{y_1'(x)}{F(x) - y_1(x)} dx \end{aligned}$$

$$\begin{aligned} &= \ln \left| \frac{F(-e-2) - y_1(-e-2)}{F(0) - y_1(0)} \right| \\ & \quad + \int_0^{-e-2} \frac{y_1'(x)}{F(x) - y_1(x)} dx \\ &= \ln \left| \frac{F(-e-2) - y_1(-e-2)}{F(-e-2) - y_1(0)} \right| \\ & \quad + \ln \left| \frac{F(-e-2) - y_1(0)}{F(0) - y_1(0)} \right| \\ & \quad + \int_0^{-e-2} \frac{y_1'(x)}{F(x) - y_1(x)} dx \\ &= \int_0^{-e-2} \frac{-y_1'(x)}{F(-e-2) - y_1(x)} dx \\ & \quad + \ln \left| \frac{y_1(0) - F(-e-2)}{y_1(0)} \right| \\ & \quad + \int_0^{-e-2} \frac{y_1'(x)}{F(x) - y_1(x)} dx \\ &= \int_0^{-e-2} \frac{y_1'(x) (F(-e-2) - F(x))}{(F(-e-2) - y_1(x)) (F(x) - y_1(x))} dx \\ & \quad + \ln \left| \frac{y_1(0) - F(-e-2)}{y_1(0)} \right| \\ &= \int_0^{-e-2} \frac{g(x) (F(-e-2) - F(x))}{(F(-e-2) - y_1(x)) (F(x) - y_1(x))^2} dx \\ & \quad + \ln \left| \frac{y_1(0) - F(-e-2)}{y_1(0)} \right|. \end{aligned}$$

Further,

$$\begin{aligned} & \int_{\widehat{C_2E_2}} F'(x)dt - \int_{\widehat{C_1E_1}} F'(x)dt \\ &= \ln \left| \frac{y_2(0) - F(-e-2)}{y_2(0)} \right| \\ & \quad - \ln \left| \frac{y_1(0) - F(-e-2)}{y_1(0)} \right| \\ & \quad + \int_0^{-e-2} g(x) (F(-e-2) - F(x)) \\ & \quad \left(\frac{1}{(F(-e-2) - y_2(x)) (F(x) - y_2(x))^2} \right. \\ & \quad \left. - \frac{1}{(F(-e-2) - y_1(x)) (F(x) - y_1(x))^2} \right) dx \\ & > 0 \tag{29} \end{aligned}$$

because of $0 > F(x) - y_1(x) > F(x) - y_2(x)$ and $F(-e-2) - F(x) > 0$ for $x \in (-e-2, 0)$ which

implies that

$$\frac{y_2(0) - F(-e - 2)}{y_2(0)} > \frac{y_1(0) - F(-e - 2)}{y_1(0)} > 0$$

and

$$0 > \frac{1}{(F(-e - 2) - y_2(x))(F(x) - y_2(x))^2} > \frac{1}{(F(-e - 2) - y_1(x))(F(x) - y_1(x))^2}.$$

Similarly, we have

$$\int_{\widehat{G_2A_2}} F'(x)dt - \int_{\widehat{G_1A_1}} F'(x)dt > 0. \tag{30}$$

Using $p = F(x)$ to rewrite system (21) in the region $\{(x, y) \in \mathbb{R}^2 | x > 0\}$ is as the following form

$$\frac{dy}{dp} = \frac{d_r p}{t_r^2(p - y)}, \quad p \in (0, +\infty). \tag{31}$$

Further, with a coordinate transformation $p \rightarrow \mu p, y \rightarrow \mu y$ with $\mu = y_{B_1}/y_{B_2}, A_2B_2C_2$ be an orbit segment which crosses through B_1 of system (31), i.e., $\widehat{A_1B_1C_1}$. Therefore, we have

$$\int_{\widehat{A_2B_2C_2}} F'(x)dt - \int_{\widehat{A_1B_1C_1}} F'(x)dt = 0. \tag{32}$$

Consider the following system without switching lines

$$\begin{aligned} \frac{dx}{dt} &= t_l(x + e + 2) - t_r e - 2t_c - y := \overline{F}(x) - y, \\ \frac{dy}{dt} &= d_l(x + e + 2) - d_r e - 2d_c := \overline{g}(x), \end{aligned} \tag{33}$$

where $\{(x, y) \in \mathbb{R}^2 | x < 0\}$. Evidently, system (21) and system (33) are the same in the region $\{(x, y) \in \mathbb{R}^2 | (d_r/d_l - 1)e + 2d_c/d_l - 2 < x < -e - 2\}$. For simplicity, we turn to study two orbit segments $\widehat{E_2F_2G_2}$ and $\widehat{E_1F_1G_1}$ in system (33), as shown in Fig. 12b, where P_i and Q_i represent the first intersection point of the orbit segment $\widehat{E_iF_iG_i}$ and y -axis for $i = 1, 2$ as t decreases and increases, respectively. On the one hand, proceeding as in the proof of $\int_{\widehat{A_2B_2C_2}} F'(x)dt = \int_{\widehat{A_1B_1C_1}} F'(x)dt$ in system (21), we can also obtain that

$$\int_{\widehat{P_2F_2Q_2}} F'(x)dt = \int_{\widehat{P_1F_1Q_1}} F'(x)dt \tag{34}$$

in system (33). On the other hand, we have

$$\int_{\widehat{P_2E_2}} \overline{F}'(x)dt - \int_{\widehat{P_1E_1}} \overline{F}'(x)dt$$

$$\begin{aligned} &= \int_0^{-e-2} \frac{\overline{F}'(x)}{\overline{F}(x) - \overline{y_2}(x)} dx \\ &\quad - \int_0^{-e-2} \frac{\overline{F}'(x)}{\overline{F}(x) - \overline{y_1}(x)} dx \\ &= \int_0^{-e-2} \frac{\overline{F}'(x)(\overline{y_2}(x) - \overline{y_1}(x))}{(\overline{F}(x) - \overline{y_1}(x))(\overline{F}(x) - \overline{y_2}(x))} dx < 0, \end{aligned} \tag{35}$$

where $\overline{y_1}(x)$ and $\overline{y_2}(x)$ represent the orbit segments $\widehat{P_1E_1}$ and $\widehat{P_2E_2}$ which lie above $y = \overline{F}(x)$, respectively. Denote $\overline{z_1}(x)$ and $\overline{z_2}(x)$ as the orbit segments $\widehat{G_1Q_1}$ and $\widehat{G_2Q_2}$ which lie below $y = \overline{F}(x)$, respectively. We can similarly obtain

$$\int_{\widehat{G_2Q_2}} F'(x)dt - \int_{\widehat{G_1Q_1}} F'(x)dt < 0. \tag{36}$$

It follows from (34), (35) and (36) that

$$\int_{\widehat{E_2F_2G_2}} F'(x)dt - \int_{\widehat{E_1F_1G_1}} F'(x)dt > 0. \tag{37}$$

In conclusion, we proved (28) by (29), (30), (32) and (37). The next thing to do in the proof is to discuss the existence of large limit cycles of system (21) by the following two cases.

Case (a) system (21) exhibits a unique small limit cycle, which is stable.

Case (b) system (21) exhibits no small limit cycles.

Consider **Case (a)**. Note that system (21) exhibits a unique small limit cycle. Denote as γ_1 . Since γ_1 is stable, we have $\oint_{\gamma_1} F'(x)dt < 0$. Combining the stability of γ_1 and (28), we can directly obtain that system (21) exhibits at most two large limit cycles. Assume that system (21) exhibits two large limit cycles γ_2 and γ_3 , where γ_2 lies in the interior of γ_3 . Moreover, we have

$$\oint_{\gamma_2} F'(x)dt = 0, \quad \oint_{\gamma_3} F'(x)dt > 0.$$

In other words, γ_2 is semi-stable and γ_3 is unstable. We claim that the assumption is invalid. For $a_1 < a_2$, we can calculate

$$\begin{aligned} &\left| \frac{F(x)|_{t_c=a_1 - y} g(x)}{F(x)|_{t_c=a_2 - y} g(x)} \right| \\ &= \begin{cases} 0, & \text{for } x > -e, \\ (x + e)g(x)(a_1 - a_2) < 0, & \text{for } -e - 2 \leq x \leq -e, \\ -2g(x)(a_1 - a_2) < 0, & \text{for } \frac{\alpha}{d_l} \\ & -e - 2 < x < -e - 2, \end{cases} \end{aligned}$$

where equality clearly cannot hold for entire closed orbit of system (21). Thus, the vector field $(F(x) - y, g(x))$ of system (21) is rotated about t_c by [22, Definition 1.6] or Definition 3.3 of [41, Chapter 4]. By Theorem 3.4 of [41, Chapter 4], the semi-stable limit cycle γ_2 will bifurcate into at least one unstable large limit cycle γ_{21} and one stable large limit cycle γ_{22} , when t_c varies in the suitable direction. It implies that there are at least three large limit cycles. This is a contradiction. Suppose that system (21) exhibits one large limit cycle γ_4 . We claim that γ_4 is unstable. Otherwise, γ_4 is stable or semi-stable. If γ_4 is stable, then there exists an large limit cycle that is unstable by the Poincaré–Bendixson theorem between γ_1 and γ_4 . This is contradictory. If γ_4 is semi-stable, then system (21) exhibits at least two large limit cycles when t_c varies in the suitable direction. This is a contradiction. The assertion is proved. In conclusion, system (21) has at most one large limit cycle in the **Case (a)**. Moreover, the large limit cycle is unstable if it exists.

Consider **Case (b)**. Notice that O of system (21) is an unstable focus. Based on (28), system (21) exhibits at most three large limit cycles. Denote as Γ_1, Γ_2 and Γ_3 , where Γ_1, Γ_2 and Γ_3 are adjacent, Γ_1 is the inner most one and Γ_3 is the outer most one. Moreover, we have

$$\oint_{\Gamma_1} F'(x)dt < 0, \quad \oint_{\Gamma_2} F'(x)dt = 0, \quad \oint_{\Gamma_3} F'(x)dt > 0.$$

By the same arguments, system (21) exhibits at least four large limit cycles when t_c varies in the suitable direction. This is a contradiction. Thus, system (21) has no large limit cycles or a stable large limit cycle or two large limit cycles in the **Case (b)**, where one of the two large limit cycles is stable, the other one is unstable, and the stable one lies in the interior of the unstable one. This finishes the proof of Lemma 5.2. \square

Based on Lemma 5.1, it suffices to investigate the existence and uniqueness of homoclinic loops of system (1) with $d_c \leq 0, \alpha > -d_c, t_r^2 - 4d_r < 0$, and $t_c < t_c^*$ in \mathcal{G}_1 .

Lemma 5.3 *When $d_c \leq 0, \alpha > -d_c, t_r^2 - 4d_r < 0, t_c < t_c^*$ in \mathcal{G}_1 , system (1) has a unique homoclinic loop and a unique limit cycle when $t_c = \varphi(\alpha)$, where the function $t_c = \varphi(\alpha)$ is continuous and monotonous satisfying $\varphi(\alpha) < t_c^*$. Moreover, the homoclinic loop is unstable and the limit cycle is stable.*

Proof First of all, we prove the existence of homoclinic loops of system (21). Denote $W_{N_l}^+$ as the stable manifold of the right-hand side of N_l of system (21), and $W_{N_l}^-$ as the unstable manifold of the right-hand side of N_l of system (21). Since there is no equilibrium point at infinity in the right half plane by Lemma 4.2, the manifolds $W_{N_l}^+$ and $W_{N_l}^-$ must intersect the curve $y = F(x)$. Denote the first intersection points of $W_{N_l}^+$ and $W_{N_l}^-$ with the curve $y = F(x)$ as $A : (x_A, F(x_A))$ and $B : (x_B, F(x_B))$, respectively. It is clear that system (21) has a homoclinic loop if and only if $x_A - x_B = 0$. To prove the existence of homoclinic loops of system (21), it suffices to prove that $x_A - x_B$ has different signs for the two different cases $t_c = t_c^*$ and $t_c \rightarrow -\infty$.

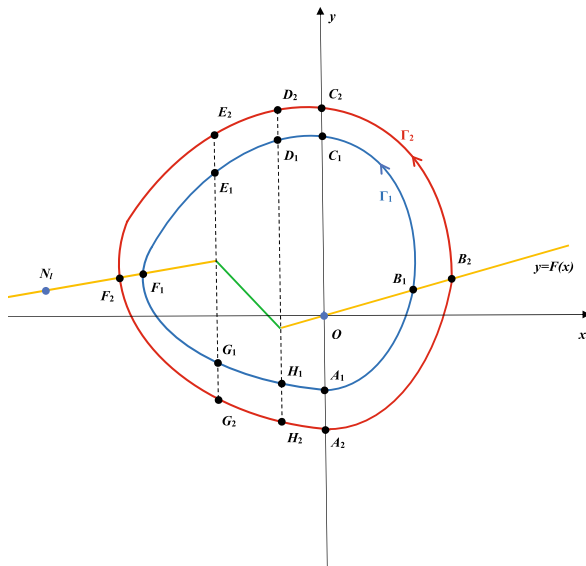
Consider $t_c = t_c^*$. It follows from statement (b) of Lemma 5.1 that system (21) exhibits neither limit cycles nor homoclinic loops, which implies $x_A - x_B \neq 0$. Note that O of system (21) is an unstable focus. We claim that $x_A - x_B < 0$, as shown in Fig. 13a. Otherwise, there exists at least one limit cycle by the Poincaré–Bendixson theorem, which contradicts the nonexistence of limit cycles of system (21). The assertion of $x_A - x_B < 0$ is proved.

Consider $t_c \rightarrow -\infty$. Define $M : (-e - 2, F(-e - 2))$ as the intersection point of the curve $y = F(x)$ and the left switching line $\Gamma_{\hat{r}}$, and P (resp. Q) be the first intersection point of the positive (resp. negative) orbit passing through M and the curve $y = F(x)$. Note that there is no equilibrium point at infinity in the right half plane by Lemma 4.2. Therefore, when $t_c \rightarrow -\infty$, we obtain that P lies on the right-hand side of Q , as shown in Fig. 13b. According to the continuous dependence of the solution on parameters and initial values, it follows that A also lies on the right-hand side of B . In other words, $x_A - x_B > 0$, as shown in Fig. 13b.

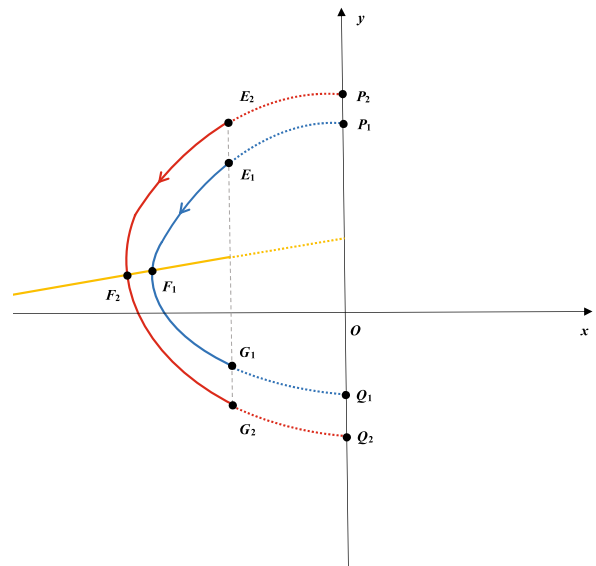
By the aforementioned discussion and the continuous dependence of the solution on parameters and the mean value theorem, there are some values $t_c \in (-\infty, t_c^*)$ so that $x_A - x_B = 0$ for system (21), as shown in Fig. 13c. Therefore, we proved the existence of homoclinic loops of system (21).

Secondly, we show the uniqueness of homoclinic loops of system (21). We claim that the manifolds $W_{N_l}^+$ and $W_{N_l}^-$ of N_l of system (21) rotate clockwise when t_c increases and $t_r, t_l, d_r, d_c, d_l, \alpha$ are fixed. For simplicity, by the transformation

$$x \rightarrow x, \quad y \rightarrow y + \widehat{F}(x),$$



(a) Assume two large limit cycles of system (21)



(b) $\widehat{E_2F_2G_2}$ and $\widehat{E_1F_1G_1}$ in system (33)

Fig. 12 The discussion of large limit cycles of system (21)

system (21) is changed into

$$\frac{dx}{dt} = -y, \quad \frac{dy}{dt} = \widehat{g}(x) + f(x)y, \quad (38)$$

where

$$f(x) = \widehat{F}'(x) = \begin{cases} t_r, & \text{if } x > -e, \\ t_c, & \text{if } -e - 2 \leq x \leq -e, \\ t_l, & \text{if } x < -e - 2. \end{cases}$$

It means that O of system (21) is moved to $O_1 : (0, 0)$ of system (38), and N_1 of system (21) is moved to $N_1 : ((d_r/d_l - 1)e + 2d_c/d_l - 2, 0)$ of system (38). Obviously, system (38) is topologically equivalent to system (21), which implies that all aforementioned discussions which hold for system (21) are also available for system (38). Therefore, we can assume that system (38) exhibits a homoclinic loop for a certain value $t_c \in (-\infty, t_c^*)$, which has one intersection point P in the positive x -axis, two intersection points Q_1 (up) and Q_2 (down) in the left switching line $\Gamma_{\widehat{r}}$, and two intersection points M (up) and N (down) in the right switching line $\Gamma_{\widehat{r}}$, as shown in Fig. 13d. Fix $t_r, t_l, d_r, d_c, d_l, \alpha$ and take $t_c \rightarrow t_c + \varepsilon$, where $|\varepsilon|$ is sufficiently small. It can easily be seen that systems (38) and $(38)|_{t_c \rightarrow t_c + \varepsilon}$ are the same in the region $\{(x, y) \in \mathbb{R}^2 | x < -e - 2\}$, which means that the orbit segment $\widehat{Q_1N_1Q_2}$ will not change when we perturb the parameter t_c . Assume that the orbit segments $\widehat{MQ_1}$ and $\widehat{Q_2N}$ are changed into the orbit

segments $\widehat{M_1Q_1}$ and $\widehat{Q_2N_2}$, respectively, when we perturb the parameter t_c , where the point M_1 is below the point M , the point N_2 is below the point N , and M_1 and N_2 are the points of the orbit after perturbation starting from Q_1 and Q_2 and intersecting with the right switching line $\Gamma_{\widehat{r}}$ for the first time as t decreases and increases, respectively, as shown in Fig. 13d. We claim that $\varepsilon > 0$. We will repeat this argument briefly later on. According to the fact that systems (38) and $(38)|_{t_c \rightarrow t_c + \varepsilon}$ are the same in the region $\{(x, y) \in \mathbb{R}^2 | x > -e\}$ and the solutions of systems (38) and $(38)|_{t_c \rightarrow t_c + \varepsilon}$ satisfy the existence, uniqueness and continuity with respect to initial conditions and parameters, it follows that we can directly obtain that the orbit segments \widehat{PM} and \widehat{NP} are changed into the orbit segments $\widehat{P_1M_1}$ and $\widehat{N_2P_2}$, respectively, when we perturb the parameter t_c , where the orbit segments $\widehat{P_1M_1}$ and $\widehat{N_2P_2}$ are below the orbit segments \widehat{PM} and \widehat{NP} , respectively, and P_1 and P_2 are the points of the orbit after perturbation starting from Q_1 and Q_2 and intersecting with the positive x -axis for the first time as t decreases and increases, respectively, as shown in Fig. 13d. Moreover, by the continuous dependence of solution on initial value and parameters, the points P_1 and P_2 must exist and be in a small neighborhood of the homoclinic loop.

We now prove $\varepsilon > 0$. Set $d_1(x) := y_\varepsilon(x) - y_0(x)$, $-e - 2 \leq x \leq -e$ be the vertical distance between

the orbit segments $\widehat{M_1 Q_1}$ and $\widehat{M Q_1}$, where $y = y_\varepsilon(x)$ and $y = y_0(x)$ represent the orbit segments $\widehat{M_1 Q_1}$ and $\widehat{M Q_1}$, respectively. Then we obtain from system (38) that

$$\begin{aligned} d_1(x) &= d_1(x) - d_1(-e - 2) \\ &= \{y_\varepsilon(x) - y_0(x)\}|_{-e-2}^x \\ &= \int_{-e-2}^x \left(\frac{-\alpha + (t_c + \varepsilon)y_\varepsilon(s)}{-y_\varepsilon(s)} - \frac{-\alpha + t_c y_0(s)}{-y_0(s)} \right) ds \\ &= H_1(x) + H_2(x) \end{aligned} \tag{39}$$

for all $x \in (-e - 2, -e)$, where

$$\begin{aligned} H_1(x) &= -\varepsilon(x + e + 2), \\ H_2(x) &= \int_{-e-2}^x d_1(s)H_3(s)ds \quad \text{and} \\ H_3(x) &= \frac{-\alpha}{y_\varepsilon(s)y_0(s)}. \end{aligned}$$

It follows from (39) that

$$d_1(x)H_3(x) = H_1(x)H_3(x) + H_2(x)H_3(x),$$

which implies that

$$\frac{dH_2(x)}{dx} = H_1(x)H_3(x) + H_2(x)H_3(x). \tag{40}$$

Solving $H_2(x)$ from the first-order linear differential equation (40) by the formula of constant variation and the initial condition $H_2(-e - 2) = 0$, we have

$$H_2(x) = \int_{-e-2}^x H_1(s)H_3(s) \exp \left\{ \int_s^x H_3(\eta)d\eta \right\} ds. \tag{41}$$

Further, by (39) and (41) we have

$$\begin{aligned} d_1(x) &= H_1(x) + \int_{-e-2}^x H_1(s)H_3(s) \\ &\quad \exp \left\{ \int_s^x H_3(\eta)d\eta \right\} ds \\ &= H_1(x) - \int_{-e-2}^x H_1(s)d \\ &\quad \left(\exp \left\{ \int_s^x H_3(\eta)d\eta \right\} \right) \\ &= H_1(-e - 2) \exp \left\{ \int_{-e-2}^x H_3(\eta)d\eta \right\} \\ &\quad + \int_{-e-2}^x H_1'(s) \exp \left\{ \int_s^x H_3(\eta)d\eta \right\} ds \\ &= -\varepsilon \int_{-e-2}^x \exp \left\{ \int_s^x H_3(\eta)d\eta \right\} ds \end{aligned}$$

$$< 0 \text{ (resp. } > 0), \quad \text{if } \varepsilon > 0 \text{ (resp. } \varepsilon < 0). \tag{42}$$

Let $d_2(x) := z_\varepsilon(x) - z_0(x)$, $-e - 2 \leq x \leq -e$ be the vertical distance between the orbit segments $\widehat{Q_2 N_2}$ and $\widehat{Q_2 N}$, where $y = z_\varepsilon(x)$ and $y = z_0(x)$ represent the orbit segments $\widehat{Q_2 N_2}$ and $\widehat{Q_2 N}$, respectively. It is similar to prove that

$$\begin{aligned} d_2(x) &= -\varepsilon \int_{-e-2}^x \exp \left\{ \int_s^x H_4(\eta)d\eta \right\} ds \\ &< 0 \text{ (resp. } > 0), \quad \text{if } \varepsilon > 0 \text{ (resp. } \varepsilon < 0). \end{aligned} \tag{43}$$

for all $x \in (-e - 2, -e)$, where

$$H_4(x) = \frac{-\alpha}{z_\varepsilon(s)z_0(s)}.$$

Therefore, the assertion of $\varepsilon > 0$ is proved by (42) and (43), which means that both the stable manifold $W_{N_l}^+$ and the unstable manifold $W_{N_l}^-$ of N_l of system (21) rotate clockwise when t_c increases and $t_r, t_l, d_r, d_c, d_l, \alpha$ are fixed. Hence, we obtain the uniqueness of homoclinic loops of system (21) by the aforementioned discussion. In other words, there is a continuous and monotonous function $\varphi(\alpha)$ on t_c such that system (1) exhibits a unique homoclinic loop when $t_c = \varphi(\alpha)$, where $\varphi(\alpha) < t_c^*$.

Thirdly, we prove the stability of homoclinic loops of system (21). Although system (21) is piecewise linear and Lipschitz continuous in \mathbb{R}^2 and Theorem 3.3 of [15] holds for a system satisfying \mathcal{C}^2 , we can easily show that Theorem 3.3 of [15] holds for system (21). Regarding the saddle N_l of system (21), its eigenvalues are denoted by λ_- and λ_+ , where $\lambda_- < 0 < \lambda_+$ and $\lambda_- + \lambda_+ = t_l$. Since $t_l > 0$, the homoclinic loop of system (21) is unstable by Theorem 3.3 of [15].

Finally, we prove the coexistence of limit cycle and homoclinic loop of system (21). By the aforementioned analysis, we know that the homoclinic loop of system (21) is unstable when it exists. Recall that O of system (21) is an unstable focus. Therefore, it clear that there exists limit cycle in the interior of the homoclinic loop by the Poincaré–Bendixson theorem. According the fact that system (21) exhibits at most two limit cycles by Lemma 5.2, we claim that there exists a unique limit cycle that is stable in the interior of the homoclinic loop. Otherwise, there exist two limit cycles in the interior of the homoclinic loop. Then, the two limit cycles consist of a stable one and a semi-stable one by the Poincaré–Bendixson theorem. We know that the vector field $(F(x) - y, g(x))$ of system (21) is rotated about

t_c by the proof of Lemma 5.2. Hence, when t_c varies in the suitable direction, system (21) exhibits at least three limit cycles. This is a contradiction. The assertion is proved. Therefore, there exists a unique limit cycle that is stable in the interior of the homoclinic loop. According to Theorem 3.5 of [41, Chapter 4], it follows that the stable limit cycle lying the interior of the homoclinic loop of system (21) expands when t_c increases. So is system (1). The proof is completed. \square

We have proved the existence of limit cycles of system (1) in Lemma 5.2, and then we now can give the uniqueness of limit cycles and the exactly two limit cycles of system (1) based on Lemma 5.3, when $d_c \leq 0$, $\alpha > -d_c$, $t_r^2 - 4d_r < 0$, and $t_c < t_c^*$ in \mathcal{G}_1 .

Lemma 5.4 Consider $d_c \leq 0$, $\alpha > -d_c$, $t_r^2 - 4d_r < 0$, $t_c < t_c^*$ in \mathcal{G}_1 . There is a continuous function $t_c = \phi(\alpha)$ such that the following statements hold, where $\varphi(\alpha) < \phi(\alpha) < t_c^*$.

- (a) When $t_c \in (-\infty, \varphi(\alpha))$, system (1) exhibits a unique limit cycle, which is stable.
- (b) When $t_c \in (\varphi(\alpha), \phi(\alpha))$, system (1) exhibits exactly two limit cycles. The inner limit cycle is stable and the outer one is unstable.
- (c) When $t_c = \phi(\alpha)$, system (1) exhibits a unique limit cycle, which is semi-stable.
- (d) When $t_c \in (\phi(\alpha), t_c^*)$, system (1) exhibits no limit cycles.

Proof According to Lemma 5.3, it follows that system (1) exhibits a unique homoclinic loop that is unstable when $t_c = \varphi(\alpha)$ as shown in Fig. 14b, where the function $\varphi(\alpha; t_r, t_l, d_r, d_c, d_l)$ is a continuous and monotonous function on t_c , and $\varphi(\alpha) < t_c^*$. Denote $W_{E_l}^+$ as the stable manifold of the right-hand side of E_l of system (1), and $W_{E_l}^-$ as the unstable manifold of the right-hand side of E_l of system (1). By the proof of Lemma 5.3, we know that the manifolds $W_{E_l}^+$ and $W_{E_l}^-$ rotate clockwise when t_c increases and $t_r, t_l, d_r, d_c, d_l, \alpha$ are fixed. If the homoclinic loop breaks, then the relative location of the stable manifold $W_{E_l}^+$ and the unstable manifold $W_{E_l}^-$ will occur two cases, as shown in Fig. 14a, c, where $\varepsilon > 0$ is sufficiently small.

Firstly, we prove conclusion (a). When $t_c \in (-\infty, \varphi(\alpha))$, the relative location of the stable manifold $W_{E_l}^+$

and the unstable manifold $W_{E_l}^-$ is as shown in Fig. 14a. Hence, we can construct the outer boundary curve. Since E_r is an unstable focus, we can construct the inner boundary curve in a small neighborhood of E_r . By the Poincaré–Bendixson theorem, there exists at least one limit cycle surrounding E_r . We have known that system (1) exhibits at most two limit cycles by Lemma 5.2. Assume that there exist two limit cycles surrounding E_r . Then, the two limit cycles consist of a stable one and a semi-stable one by the Poincaré–Bendixson theorem, which leads to the conclusion that system (1) exhibits at least three limit cycles when t_c varies in the suitable direction. This is a contradiction. Hence, there exists a unique limit cycle, which is stable. Moreover, the stable limit cycle expands when t_c increases. Conclusion (a) is proven.

Secondly, we prove conclusions (b) and (c). When $t_c \in (\varphi(\alpha), +\infty)$, the relative location of the stable manifold $W_{E_l}^+$ and the unstable manifold $W_{E_l}^-$ is as shown in Fig. 14c. We have shown that system (1) exhibits a unique limit cycle that is stable in conclusion (a) when $t_c \in (-\infty, \varphi(\alpha))$; a unique limit cycle that is stable and lies in the interior of the unstable homoclinic loop in Lemma 5.3 when $t_c = \varphi(\alpha)$. Combining Lemma 5.2 and the Poincaré–Bendixson theorem, we claim that system (1) exhibits two limit cycles when $t_c \in (\varphi(\alpha), \varphi(\alpha) + \varepsilon)$, where the inner limit cycle is stable and the outer one is unstable. Otherwise, system (1) has no limit cycles when $t_c \in (\varphi(\alpha), \varphi(\alpha) + \varepsilon)$; a stable homoclinic loop when $t_c = \varphi(\alpha)$. This is contradictory. Hence, system (1) has exactly two limit cycles when $t_c \in (\varphi(\alpha), \varphi(\alpha) + \varepsilon)$. Moreover, the attracting limit cycle expands and the repelling one contracts when t_c increases. Therefore, by the continuous dependence of solutions on parameters and the mean value theorem, we further obtain that there exists a continuous function $\phi(\alpha; t_r, t_l, d_r, d_c, d_l)$ such that when $t_c = \phi(\alpha)$ system (1) exhibits a unique limit cycle that is semi-stable, where $\varphi(\alpha) < \phi(\alpha) < t_c^*$. Then, system (1) has two limit cycles when $\varphi(\alpha) < t_c < \phi(\alpha)$. Conclusions (b) and (c) are proved.

Finally, we prove conclusion (d). When $\phi(\alpha) < t_c < t_c^*$, the semi-stable limit cycle disappears. Hence, system (1) has no limit cycles. Conclusion (d) is proved. \square

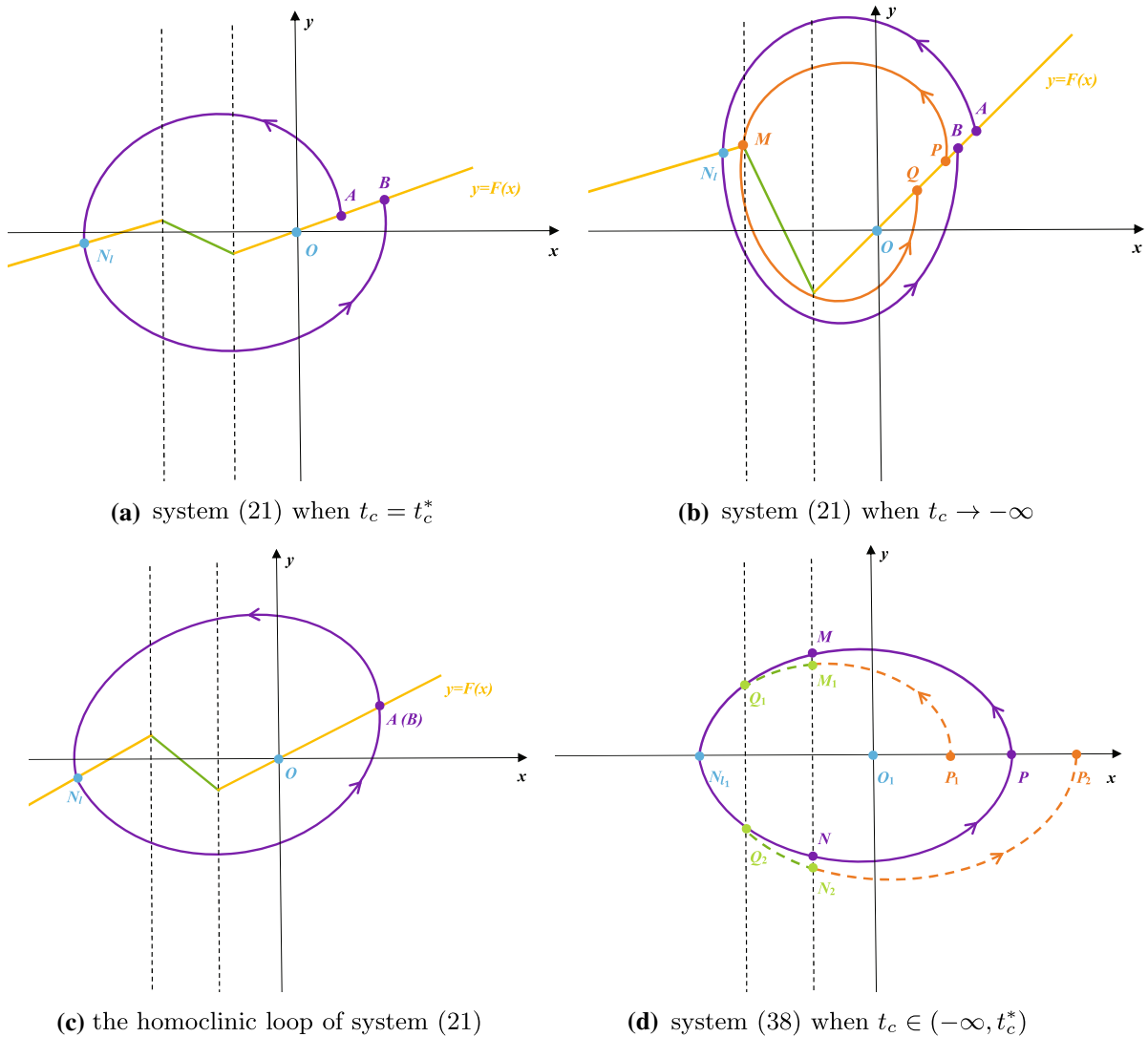


Fig. 13 The discussion of the existence and uniqueness of homoclinic loops of system (1)

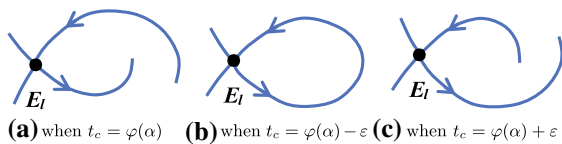


Fig. 14 The homoclinic loop bifurcation of system (1)

5.2 Limit cycles and homoclinic loops of system (1) with $d_c < 0$ and $d_c < \alpha \leq -d_c$ in \mathcal{G}_1

The following lemma is to give the nonexistence of limit cycles and homoclinic loops of system (1), when $d_c < 0$ and $d_c < \alpha \leq -d_c$ in \mathcal{G}_1 .

Lemma 5.5 *Considering $d_c < 0$, $d_c < \alpha \leq -d_c$ in \mathcal{G}_1 , system (1) exhibits neither limit cycles nor homoclinic loops, if one of the following statements holds:*

- (a) $t_r^2 - 4d_r \geq 0$;
- (b) $t_r^2 - 4d_r < 0$ and $t_c \geq 0$.

Proof Consider $t_r^2 - 4d_r \geq 0$. O of system (21) is an unstable node by Lemma 4.1, which implies that system (21) has at least one invariant line in $\mathcal{S}_{\hat{r}}$. Thus, any orbit passing the switching line $\Gamma_{\hat{r}}$ has no intersections with the switching line $\Gamma_{\hat{r}}$ again. Moreover, limit cycles of system (21) must only surround O if it exists. Thus,

system (21) exhibits neither limit cycles nor homoclinic loops. The condition (a) is proved.

Consider $t_r^2 - 4d_r < 0$ and $t_c \geq 0$. From Lemma 4.1, we know that O of system (21) is an unstable focus, N_c (resp. N_{cl}) of system (21) is a saddle if $d_c < \alpha < -d_c$ (resp. $\alpha = -d_c$). In order to study the nonexistence of limit cycles and homoclinic loops of system (21), construct an energy function along the vector field of system (21) as follows

$$E(x, y) := \int_0^x g(s)ds + \frac{y^2}{2}.$$

Then, we have

$$\frac{dE(x, y)}{dt} = g(x)F(x) > 0 \text{ (resp. } = 0),$$

$$\text{if } x \neq 0 \text{ (resp. } x = 0),$$

when $t_c \geq 0$ and $d_c < \alpha \leq -d_c$ in the region $\{(x, y) \in \mathbb{R}^2 | x \geq (d_r/d_c - 1)e\}$. We claim that system (21) exhibits neither limit cycles nor homoclinic loops in this case. Otherwise, we have

$$\oint_{\Gamma} dE = \oint_{\Gamma} g(x)F(x) > 0,$$

for any limit cycle or homoclinic loop Γ of system (21), which contradicts the fact $\oint_{\Gamma} dE = 0$. This completes the proof. \square

Based on Lemma 5.5, we give the existence and uniqueness of limit cycles and homoclinic loops of system (1), when $d_c < 0$, $d_c < \alpha \leq -d_c$, $t_r^2 - 4d_r < 0$ and $t_c < 0$ in \mathcal{G}_1 .

Lemma 5.6 Consider $d_c < 0$, $d_c < \alpha \leq -d_c$, $t_r^2 - 4d_r < 0$ and $t_c < 0$ in \mathcal{G}_1 . There is a continuous function $t_c = h(\alpha)$ such that the following statements hold, where $h(\alpha) < 0$.

- (a) System (1) exhibits a unique limit cycle that is stable if and only if $t_c < h(\alpha)$.
- (b) System (1) exhibits a stable homoclinic loop if and only if $t_c = h(\alpha)$.
- (c) System (1) exhibits neither limit cycles nor homoclinic loops if and only if $t_c > h(\alpha)$.

Proof In [31], Llibre, Ponce and Valls studied the limit cycles of the following Liénard piecewise linear differential system

$$\frac{dx}{d\tau} = \tilde{F}(x) - y, \quad \frac{dy}{d\tau} = \tilde{g}(x), \tag{44}$$

where

$$\tilde{F}(x) = \begin{cases} T_R(x - v) + T_C v, & \text{if } x > v, \\ T_C x, & \text{if } -u \leq x \leq v, \\ T_L(x + u) - T_C u, & \text{if } x < -u, \end{cases}$$

$$\tilde{g}(x) = \begin{cases} r(x - v) + v, & \text{if } x > v, \\ x, & \text{if } -u \leq x \leq v, \\ l(x + u) - u, & \text{if } x < -u, \end{cases}$$

and the constants u and v are positive. When $T_R = T_C \neq 0$ and $r = 1$, $\tilde{F}(x)$ and $\tilde{g}(x)$ of system (44) can be simplified as the following form

$$\hat{F}(x) = \begin{cases} T_R x, & \text{if } x \geq -u, \\ T_L(x + u) - T_R u, & \text{if } x < -u, \end{cases}$$

and

$$\hat{g}(x) = \begin{cases} x, & \text{if } x \geq -u, \\ l(x + u) - u, & \text{if } x < -u. \end{cases}$$

Assuming $d_r > 0$ and applying

$$T_R = \frac{t_r}{\sqrt{d_r}}, \quad T_L = \frac{t_c}{\sqrt{d_r}}, \quad l = \frac{d_c}{d_r}, \quad u = e, \tag{45}$$

we obtain that $\hat{F}(x)$ and $\hat{g}(x)$ of system (44) can be further simplified to

$$\bar{F}(x) = \begin{cases} \frac{t_r}{\sqrt{d_r}} x, & \text{if } x \geq -e, \\ \frac{t_c}{\sqrt{d_r}}(x + e) - \frac{t_r}{\sqrt{d_r}} e, & \text{if } x < -e, \end{cases}$$

and

$$\bar{g}(x) = \begin{cases} x, & \text{if } x \geq -e, \\ \frac{d_c}{d_r}(x + e) - e, & \text{if } x < -e. \end{cases}$$

By the scaling transformation $y \rightarrow y/\sqrt{d_r}$, $\tau \rightarrow \sqrt{d_r}t$, system (44) becomes

$$\frac{dx}{dt} = F(x) - y, \quad \frac{dy}{dt} = g(x), \tag{46}$$

where,

$$F(x) = \begin{cases} t_r x, & \text{if } x \geq -e, \\ t_c(x + e) - t_r e, & \text{if } x < -e, \end{cases}$$

and

$$g(x) = \begin{cases} d_r x, & \text{if } x \geq -e, \\ d_c(x + e) - d_r e, & \text{if } x < -e. \end{cases}$$

Using Lemma 4.1, we know that system (21) has two equilibrium points O and N_c when $d_c < \alpha < -d_c$; O and N_{cl} when $\alpha = -d_c > 0$. Moreover, O of system (21) is an unstable focus for $t_r^2 - 4d_r <$

0, N_c and N_{cl} of system (21) are saddles. It is clear that the above equilibrium points all lie in the region $\{(x, y) \in \mathbb{R}^2 | x \geq -e - 2\}$. Based on the index theory, limit cycle of system (21) lies in the region $\{(x, y) \in \mathbb{R}^2 | x \geq -e - 2\}$ if it exists. It is important to note that system (21) and system (46) are the same in the region $\{(x, y) \in \mathbb{R}^2 | x \geq -e - 2\}$. Moreover, systems (44) and (46) are topologically equivalent. Therefore, we can directly obtain some results of limit cycles and homoclinic loops of system (1) by using the known results of limit cycles and homoclinic loops of system (44) (see [31]).

Consider $T_R = T_C > 0, |T_C| < 2, T_L < 0, r = 1$ and $l < 0$ in system (44). By (45), we have $t_r > 0, t_c < 0, d_r > 0, d_c < 0$ and $t_r^2 - 4d_r < 0$ in system (46). System (46) has two equilibrium points, $M : (0, 0)$ and $N : ((d_r/d_c - 1)e, (t_c d_r/d_c - t_r)e)$. M of system (46) is exactly O of system (21) when $d_c < \alpha \leq -d_c$, N of system (46) is exactly N_c of system (21) when $d_c < \alpha < -d_c$; and N of system (46) is exactly N_{cl} of system (21) when $\alpha = -d_c > 0$. If $T_R = T_C > 0, |T_C| < 2, T_L < 0, r = 1$ and $l < 0$ hold, we recall that system (44) has a unique limit cycle surrounding the origin that is stable if and only if $e^{\pi\gamma} Y_+^l + Y_-^l < 0$; a stable homoclinic loop if and only if $e^{\pi\gamma} Y_+^l + Y_-^l = 0$; neither limit cycles nor homoclinic loops if and only if $e^{\pi\gamma} Y_+^l + Y_-^l > 0$ by Theorem 3 of [31], where

$$\begin{aligned} \gamma &= \frac{T_C}{\sqrt{4 - T_C^2}}, \quad \omega = \frac{\sqrt{4 - T_C^2}}{2}, \\ \sigma &= \frac{T_C}{2}, \quad \delta_{\pm} = \frac{T_L \pm \sqrt{T_L^2 - 4l}}{2l}, \\ \psi_{\pm} &= 2 \cdot \arctan \left(\frac{\omega}{\sqrt{(\sigma - \delta_{\pm})^2 + \omega^2} \pm (\sigma - \delta_{\pm})} \right), \\ Y_{\pm}^l &= \pm u \cdot \exp(\pm\gamma\psi_{\pm}) \sqrt{(\sigma - \delta_{\pm})^2 + \omega^2}. \end{aligned}$$

Therefore, if $t_r > 0, t_c < 0, d_r > 0, d_c < 0$ and $t_r^2 - 4d_r < 0$ hold, system (46) exhibits a unique limit cycle that is stable surrounding the origin if and only if $e^{\pi\gamma} Y_+^l + Y_-^l < 0$; a stable homoclinic loop if and only if $e^{\pi\gamma} Y_+^l + Y_-^l = 0$; neither limit cycles nor homoclinic loops if and only if $e^{\pi\gamma} Y_+^l + Y_-^l > 0$, where

$$\begin{aligned} \gamma &= \frac{t_r}{\sqrt{4d_r - t_r^2}}, \quad \omega = \frac{\sqrt{4d_r - t_r^2}}{2\sqrt{d_r}}, \\ \sigma &= \frac{t_r}{2\sqrt{d_r}}, \quad \delta_{\pm} = \sqrt{d_r} \cdot \frac{t_c \pm \sqrt{t_c^2 - 4d_c}}{2d_c}, \end{aligned}$$

$$\begin{aligned} \psi_{\pm} &= 2 \cdot \arctan \left(\frac{\omega}{\sqrt{(\sigma - \delta_{\pm})^2 + \omega^2} \pm (\sigma - \delta_{\pm})} \right), \\ Y_{\pm}^l &= \pm e \cdot \exp(\pm\gamma\psi_{\pm}) \sqrt{(\sigma - \delta_{\pm})^2 + \omega^2}. \end{aligned}$$

Besides, for $a_1 < a_2$, we can compute

$$\begin{aligned} &\left| \begin{matrix} F(x)|_{t_c=a_1} - y g(x) \\ F(x)|_{t_c=a_2} - y g(x) \end{matrix} \right| \\ &= \begin{cases} = 0, & \text{for } x \geq -e, \\ (x + e)g(x)(a_1 - a_2) < 0, & \text{for } x < -e, \end{cases} \end{aligned}$$

where equality clearly cannot hold for entire closed orbit of system (46). Hence, the vector field $(F(x) - y, g(x))$ of system (46) is rotated about t_c by [22, Definition 1.6] or Definition 3.3 of [41, Chapter 4]. This implies the result. \square

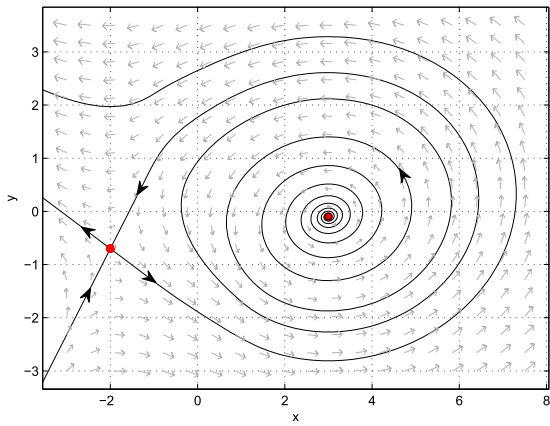
6 Proofs of Theorems 2.1–2.6

Proof of Theorem 2.1 It follows from Lemma 4.1 that system (1) exhibits a continuum of non-isolated equilibrium points CE when $\alpha = 0$ in \mathcal{G}_{11} . If $\alpha = \varepsilon$ and $\varepsilon > 0$ is small, CE will vanish and an unstable focus E_r and a saddle E_l will appear. Moreover, it is evident that there is no limit cycle by the qualitative property of CE . Therefore, DB_1 and DB_2 are degenerate boundary equilibrium bifurcation curves.

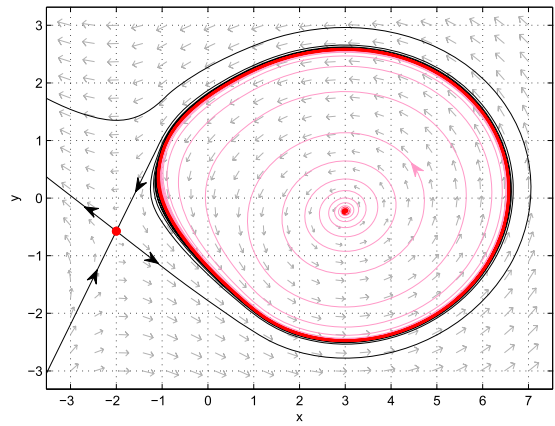
Applying Lemma 5.3, we know that system (1) exhibits a unique homoclinic loop that is unstable when $\alpha > 0$ and $t_c = \varphi(\alpha)$ in \mathcal{G}_{11} , where the function $\varphi(\alpha)$ is a continuous and monotonous function on t_c and $\varphi(\alpha) < t_c^*$. Therefore, homoclinic bifurcation curve HL is obtained.

According to Lemma 5.4, it follows that system (1) exhibits a unique limit cycle that is semi-stable when $\alpha > 0$ and $t_c = \phi(\alpha)$ in \mathcal{G}_{11} , where $\phi(\alpha)$ is a continuous on t_c and $\varphi(\alpha) < \phi(\alpha) < t_c^*$. If $\alpha > 0, t_c = \phi(\alpha) + \varepsilon$ and $\varepsilon > 0$ (ε is small), the semi-stable limit cycle will vanish. However, there are two limit cycles accompanied by the vanish of the semi-stable limit cycle if $\varepsilon < 0$. Hence, DL is called as double limit cycle bifurcation curve.

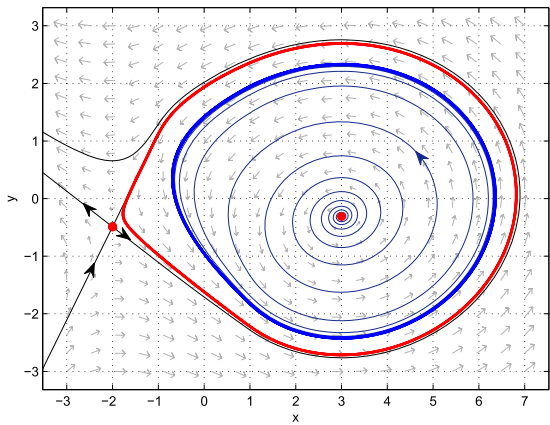
By the aforementioned discussion and Lemma 4.2, we obtain that there is no limit cycle when parameters belong to the region I (see Fig. 1b for its global phase portraits in the Poincaré disc) or II (see Fig. 1c for its global phase portraits in the Poincaré disc); one stable limit cycle when parameters belong to the region III



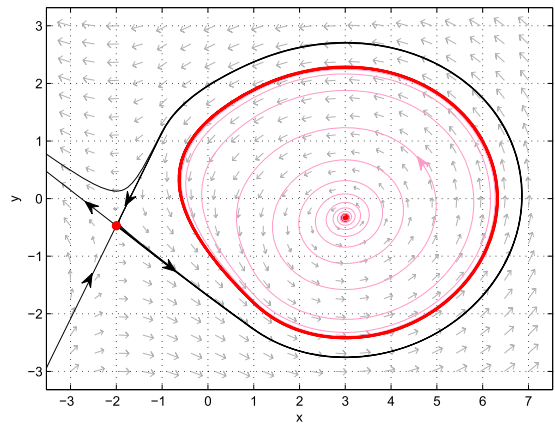
(a) when $(\alpha, t_c) = (1, -0.3)$



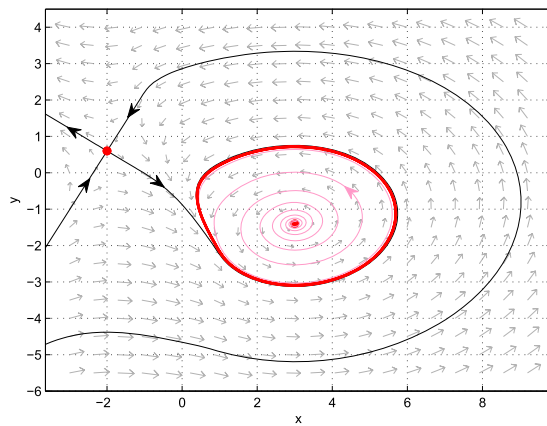
(b) when $(\alpha, t_c) = (1, -0.426)$



(c) when $(\alpha, t_c) = (1, -0.51)$



(d) when $(\alpha, t_c) = (1, -0.5285)$



(e) when $(\alpha, t_c) = (1, -1.6)$

Fig. 15 Numerical phase portraits of system (1) with $(t_r, t_l, d_r, d_c, d_l) = (0.1, 1, 0.5, 0, -1) \in \mathcal{G}_{11}$

(see Fig. 1d for its global phase portraits in the Poincaré disc); two limit cycles when parameters belong to the region IV (see Fig. 1e for its global phase portraits in the Poincaré disc). This completes the proof. \square

Proof of Theorem 2.2 Proceeding as in the proof of Theorem 2.1, we have the degenerate boundary equilibrium bifurcation curves DB_1 and DB_2 in \mathcal{G}_{12} . By Lemma 4.1, system (1) exhibits no equilibrium point when $\alpha < 0$ in \mathcal{G}_{12} ; two equilibrium points E_l and E_r when $\alpha > 0$ in \mathcal{G}_{12} , where E_l is a saddle, E_r is an unstable node. Hence, system (1) has no limit cycles.

Based on the aforementioned discussion and Lemma 4.2, we obtain the global phase portraits in the Poincaré disc of the regions V (see Fig. 2b) and VI (see Fig. 2c). The proof is completed. \square

Remark 5 Since the proof of Theorem 2.4 is similar with the proof of Theorem 2.1 and the proofs of Theorems 2.3, 2.5 and 2.6 are similar with the proof of Theorem 2.2, we omit the corresponding proofs.

7 Numerical results

In order to illustrate our theoretical results, we give some numerical phase portraits of system (1). Let $(t_r, t_l, d_r, d_c, d_l) = (0.1, 1, 0.5, 0, -1) \in \mathcal{G}_{11}$. By numerical simulations, system (1) exhibits no limit cycles for $(\alpha, t_c) = (1, -0.3)$ (see Fig. 15a); one semi-stable limit cycle for $(\alpha, t_c) = (1, -0.426)$ (see Fig. 15b); two limit cycles for $(\alpha, t_c) = (1, -0.51)$ (see Fig. 15c); one unstable homoclinic loop and one stable limit cycle for $(\alpha, t_c) = (1, -0.5285)$ (see Fig. 15d); and one stable limit cycle for $(\alpha, t_c) = (1, -1.6)$ (see Fig. 15e).

Set $(t_r, t_l, d_r, d_c, d_l) = (0.1, 1, 0.5, -0.1, -1) \in \mathcal{G}_{14}$. By numerical simulations, system (1) exhibits no limit cycles for $(\alpha, t_c) = (1, -0.3)$ (see Fig. 16a); one semi-stable limit cycle for $(\alpha, t_c) = (1, -0.476)$ (see Fig. 16b); two limit cycles for $(\alpha, t_c) = (1, -0.5)$ (see Fig. 16c); one unstable homoclinic loop and one stable limit cycle for $(\alpha, t_c) = (1, -0.55)$ (see Fig. 16d); and one stable limit cycle for $(\alpha, t_c) = (1, -1)$ (see Fig. 16e). And system (1) has no limit cycles for $(\alpha, t_c) = (0, -0.1)$ (see Fig. 16f); one homoclinic loop for $(\alpha, t_c) = (0, -0.12799)$ (see Fig. 16g); and one stable limit cycle for $(\alpha, t_c) = (0, -0.3)$ (see Fig. 16h).

8 Concluding remarks

In this section, we compare the global dynamics and techniques of this paper to those of known papers. Based on all results in this paper, global phase portraits in the Poincaré disc and the bifurcation diagram of system (1) were given completely for the case $t_r t_l > 0, d_r d_l < 0, d_c \leq 0$.

When $t_r t_l > 0$ and $d_r d_l > 0$, the global dynamics of system (1) are completely different compared with this paper, see [12, 31, 35] and references therein. For example, consider system (1) with $t_r t_l > 0, d_r > 0, d_c > 0, d_l > 0$, and then system (1) has a unique equilibrium point that lies in an open linear zone or a switching line. However, the results of this paper for the finite equilibrium point are utterly different and more complex, where system (1) has two isolated equilibrium points for $\alpha > d_c$; one equilibrium point (one continuum of non-isolated equilibrium point as $d_c = 0$ or one isolated equilibrium point as $d_c < 0$) for $\alpha = d_c$; no equilibrium point for $\alpha < d_c$, see Lemma 4.1 for more descriptions. Naturally, the global phase portraits and bifurcations of system (1) in this paper are completely different from those of system (1) with $t_r t_l > 0, d_r > 0, d_c > 0, d_l > 0$. Since $d_r d_l < 0$, it means that the dynamic of the one of the exterior linear zones is saddle and the remaining one is anti-saddle. Therefore, the results of this paper have the special dynamical behavior that is the coexistence of limit cycle and homoclinic loop.

Llibre et al. [31] proved the existence and uniqueness of homoclinic loop involving two linear zones for system (1) with some restrictions. In this paper, we show the existence and uniqueness of homoclinic loop involving three linear zones for system (1) by using new techniques. To explain why, we recall the techniques used to prove the existence and uniqueness of homoclinic loop in [31]. When $t_l = t_c, d_l = d_c$ or $t_r = t_c, d_r = d_c$ system (1) becomes a continuous piecewise linear system with only two different linear zones. Without loss of generality, we consider the case $t_l = t_c, d_l = d_c$ and then system (1) becomes

$$\frac{dx}{dt} = F(x) - y, \quad \frac{dy}{dt} = g(x) - \alpha, \tag{47}$$

where

$$F(x) = \begin{cases} t_r(x - 1) + t_c, & \text{if } x > 1, \\ t_c x, & \text{if } x \leq 1, \end{cases}$$

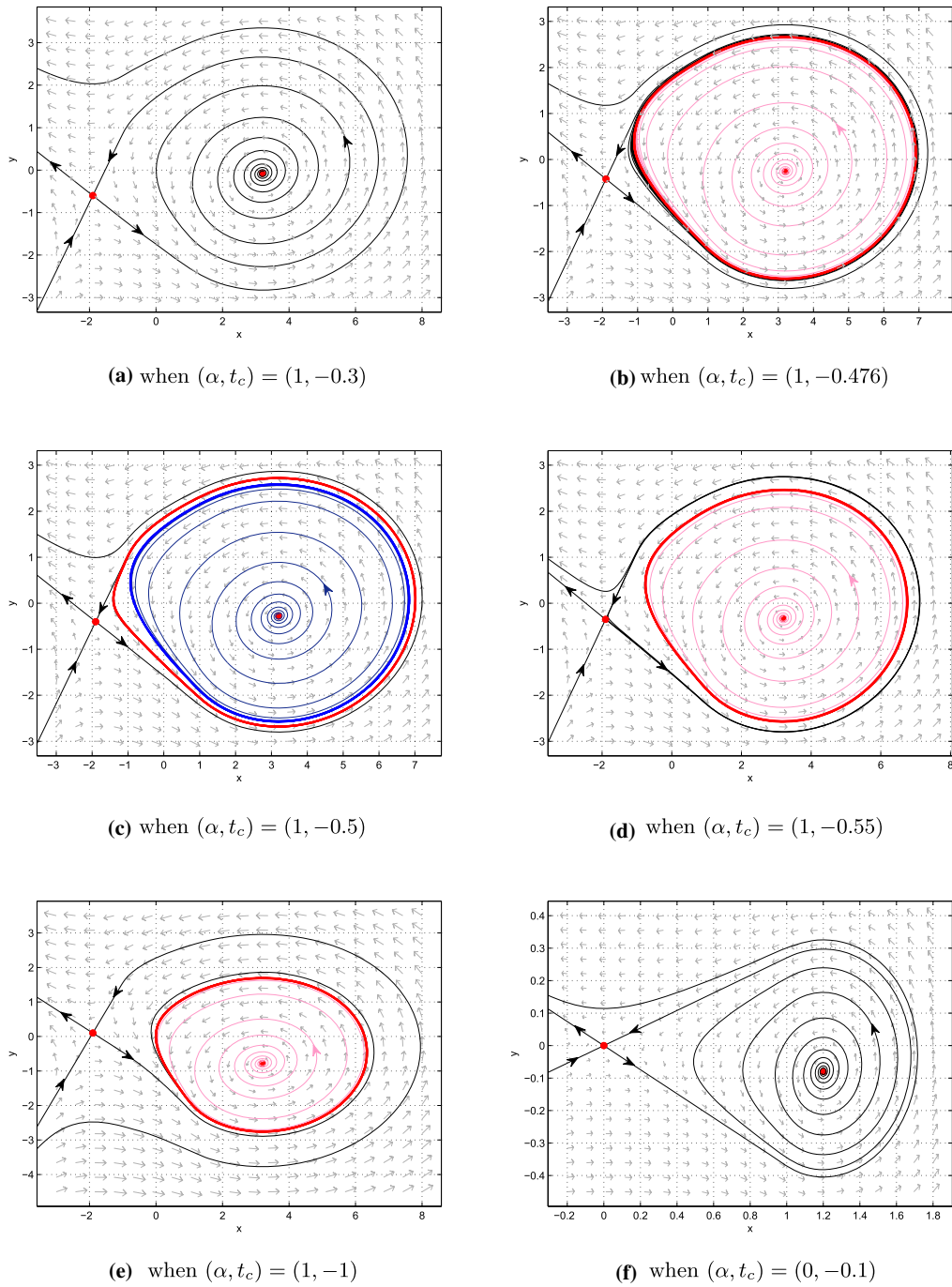
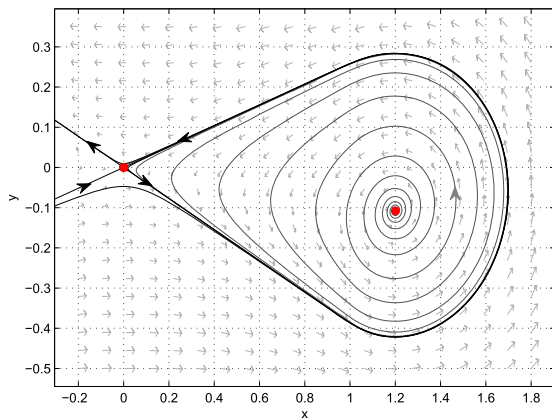
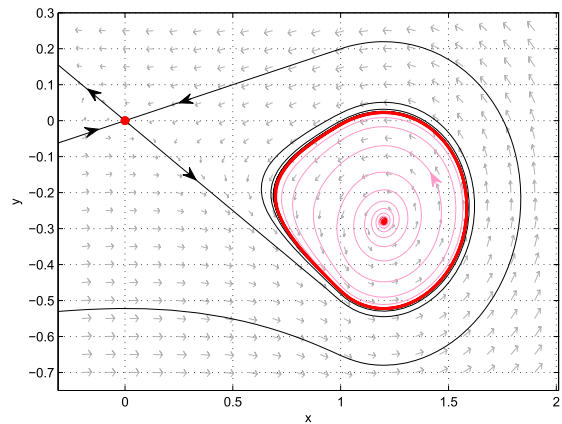


Fig. 16 Numerical phase portraits of system (1) with $(t_r, t_l, d_r, d_c, d_l) = (0.1, 1, 0.5, -0.1, -1) \in \mathcal{G}_{14}$



(g) when $(\alpha, t_c) = (0, -0.12799)$



(h) when $(\alpha, t_c) = (0, -0.3)$

Fig. 16 continued

and

$$g(x) = \begin{cases} d_r(x - 1) + d_c, & \text{if } x > 1, \\ d_c x, & \text{if } x \leq 1. \end{cases}$$

Without loss of generality, consider system (47) with $t_r < 0, 0 < t_c < 2, d_r < 0, d_c > 0, \alpha < d_c$, see the section 4 of [31] for more descriptions. Firstly, they computed the stable manifold and the unstable manifold of the left-hand side of saddle point of system (47) by the Jacobian matrix of saddle point. Let A and B be the intersection points of the stable manifold and the unstable manifold of the left-hand side of saddle point with the switching line $x = 1$, respectively. Secondly, they calculated the orbits γ_1 and γ_2 starting from A and B in the region $\{(x, y) \in \mathbb{R}^2 | x < 1\}$, respectively. Finally, they obtained the conclusion of the existence and uniqueness of homoclinic loop for system (47) if γ_1 and γ_2 intersect each other.

Now, look at the problems we face. Without loss of generality, consider system (1) with $d_r > 0, d_c \leq 0, d_l < 0, t_r > 0, t_c < t_c^*, t_l > 0, \alpha > -d_c$ and $t_r^2 - 4d_r < 0$. It then follows from Lemma 4.1 that system (1) has two equilibrium points E_l and E_r , which are lie in \mathcal{S}_l and \mathcal{S}_r , respectively. Since E_l is a saddle, the homoclinic loop involves three linear zones if it exists. Although we know that the dynamics of the left and right linear zones of system (1) are saddle and focus respectively, it is quite difficult to study the existence and uniqueness of homoclinic loop involving three linear zones by the above techniques because of complex computations. In other words, we have to

adopt new techniques to solve our face problems, see Lemma 5.3 for more descriptions. Denote the first intersection points of the stable manifold and the unstable manifold of the right-hand side of saddle point of system (1) with the curve $y = F(x)$ as $A : (x_A, F(x_A))$ and $B : (x_B, F(x_B))$, respectively. First, we prove that $x_A - x_B < 0$ for $t_c = t_c^*$ and $x_A - x_B > 0$ for $t_c \rightarrow -\infty$. By the zero point theorem, we obtain the existence of homoclinic loop of system (1), i.e., $x_A - x_B = 0$ for some values t_c . Second, we show that the stable manifold and the unstable manifold of the right-hand side of saddle point of system (1) rotate clockwise when t_c increases and $t_r, t_l, d_r, d_c, d_l, \alpha$ are fixed. Therefore, we know that the homoclinic loop of system (1) is unique if it exists. By the aforementioned two steps, we give the existence and uniqueness of homoclinic loop. Finally, we prove the coexistence of limit cycle and the above homoclinic loop by reduction to absurdity, see Lemma 5.3 for more descriptions.

Acknowledgements The authors are very grateful to the anonymous reviewers for their valuable comments and suggestions that greatly improve the presentation and mathematics of this paper. The paper is supported partially by the National Natural Science Foundation of China (No. 62173092, 12171485).

Funding The paper is supported by the National Natural Science Foundation of China (Nos. 62173092, 12171485).

Data availability All data, models and code generated or used during the study appear in the submitted article.

Declarations

Conflict of interest This manuscript has not been published and is not under consideration for publication elsewhere. All the authors have approved the manuscript and agree with this submission.

References

- Bonsel, J.H., Fey, R.H.B., Nijmeijer, H.: Application of a dynamic vibration absorber to a piecewise linear beam system. *Nonlinear Dyn.* **37**, 227–243 (2004)
- Borghetti, J., Snider, G.S., Kuekes, P.J., Jang, J.J., Stewart, D.R., Williams, R.S.: ‘Memristive’ switches enable ‘stateful’ logic operations via material implication. *Nature* **468**, 873–876 (2010)
- Cao, Q., Wiercigroch, M., Pavlovskaja, E.E., Grebogi, C., Thompson, J.M.T.: Archetypal oscillator for smooth and discontinuous dynamics. *Phys. Rev. E* **74**, 046218–046222 (2006)
- Cao, Q., Wiercigroch, M., Pavlovskaja, E.E., Grebogi, C., Thompson, J.M.T.: The limit case response of the archetypal oscillator for smooth and discontinuous dynamics. *Int. J. Nonlinear Mech.* **43**, 462–473 (2008)
- Cao, Q., Wiercigroch, M., Pavlovskaja, E.E., Thompson, J.M.T., Grebogi, C.: Piecewise linear approach to an archetypal oscillator for smooth and discontinuous dynamics. *Philos. Trans. R. Soc. A* **366**, 635–652 (2008)
- Cao, Q., Han, Y., Liang, T.: Multiple buckling and codimension-three bifurcation phenomena of a nonlinear oscillator. *Int. J. Bifurc. Chaos* **24**(1430005), 1–17 (2014)
- Carmona, V., Freire, E., Ponce, E., Torres, F.: On simplifying and classifying piecewise linear systems. *IEEE Trans. Circuits Syst.* **I**(49), 609–620 (2002)
- Chen, H.: Global dynamics of memristor oscillators. *Int. J. Bifurc. Chaos* **26**(1650198), 1–29 (2016)
- Chen, H., Li, X.: Global phase portraits of memristor oscillators. *Int. J. Bifurc. Chaos* **24**(1450152), 1–31 (2014)
- Chen, H., Tang, Y.: At most two limit cycles in a piecewise linear differential system with three zones and asymmetry. *Physica D* **386–387**, 23–30 (2019)
- Chen, H., Tang, Y.: A proof of Euzébio–Pazim–Ponce’s conjectures for a degenerate planar piecewise linear differential system with three zones. *Physica D* **401**(132150), 1–22 (2020)
- Chen, H., Li, D., Xie, J., Yue, Y.: Limit cycles in planar continuous piecewise linear systems. *Commun. Nonlinear Sci. Numer. Simul.* **47**, 438–454 (2017)
- Chen, H., Wei, F., Xia, Y., Xiao, D.: Global dynamics of an asymmetry piecewise linear differential system: theory and applications. *Bull. Sci. Math.* **160**(102858), 1–43 (2020)
- Chen, H., Jia, M., Tang, Y.: A degenerate planar piecewise linear differential system with three zones. *J. Differ. Equ.* **297**, 433–468 (2021)
- Chow, S.-N., Li, C., Wang, D.: *Normal Forms and Bifurcation of Planar Vector Fields*. Cambridge Press, Cambridge (1994)
- Chua, L.O.: Memristor: the missing circuit element. *IEEE Trans. Circuit Theory* **CT-18**, 507–519 (1971)
- Corinto, F., Ascoli, A., Gilli, M.: Nonlinear dynamics of memristor oscillators. *IEEE Trans. Circuits Syst. I: Regul. Pap.* **58**, 1323–1336 (2011)
- di Bernardo, M., Budd, C.J., Champneys, A.R., Kowalczyk, P.: *Piecewise-Smooth Dynamical Systems: Theory and Applications*. Springer, London (2008)
- Euzébio, R., Pazim, R., Ponce, E.: Jump bifurcations in some degenerate planar piecewise linear differential systems with three zones. *Physica D* **325**, 74–85 (2016)
- Freire, E., Ponce, E., Rodrigo, F., Torres, F.: Bifurcation sets of continuous piecewise linear systems with two zones. *Int. J. Bifurc. Chaos* **8**, 2073–2097 (1998)
- Freire, E., Ponce, E., Rodrigo, F., Torres, F.: Bifurcation sets of symmetrical continuous piecewise linear systems with three zones. *Int. J. Bifurc. Chaos* **12**, 1675–1702 (2002)
- Han, M.: Global behavior of limit cycles in rotated vector fields. *J. Differ. Equ.* **151**, 20–35 (1999)
- Han, Y., Cao, Q., Chen, Y., Wiercigroch, M.: A novel smooth and discontinuous oscillator with strong irrational nonlinearities. *Sci. China Phys. Mech. Astron.* **55**, 1832–1843 (2012)
- Itoh, M., Chua, L.O.: Memristor oscillator. *Int. J. Bifurc. Chaos* **18**, 3183–3206 (2008)
- Li, S., Llibre, J.: Phase portraits of piecewise linear continuous differential systems with two zones separated by a straight line. *J. Differ. Equ.* **266**, 8094–8109 (2019)
- Li, S., Liu, C., Llibre, J.: The planar discontinuous piecewise linear refracting systems have at most one limit cycle. *Nonlinear Anal. Hybrid Syst.* **41**, 101045 (2021)
- Llibre, J., Sotomayor, J.: Phase portraits of planar control systems. *Nonlinear Anal.* **27**, 1177–1197 (1996)
- Llibre, J., Teixeira, M.A.: Piecewise linear differential systems with only centers can create limit cycles? *Nonlinear Dyn.* **91**, 249–255 (2018)
- Llibre, J., Teruel, A.E.: *Introduction to the Qualitative Theory of Differential Systems: Planar, Symmetric and Continuous Piecewise Linear Systems*. Birkhäuser Advanced Texts, Berlin (2014)
- Llibre, J., Ordóñez, M., Ponce, E.: On the existence and uniqueness of limit cycles in planar continuous piecewise linear systems without symmetry. *Nonlinear Anal. Real World Appl.* **14**, 2002–2012 (2013)
- Llibre, J., Ponce, E., Valls, C.: Uniqueness and non-uniqueness of limit cycles for piecewise linear differential systems with three zones and no symmetry. *J. Nonlinear Sci.* **25**, 861–887 (2015)
- Llibre, J., Ponce, E., Valls, C.: Two limit cycles in Liénard piecewise linear differential systems. *J. Nonlinear Sci.* **29**, 1499–1522 (2019)
- McKean, H.P.: Nagumo’s equation. *Adv. Math.* **4**, 209–223 (1970)
- McKean, H.P.: Stabilization of solutions of a caricature of the Fitzhugh–Nagumo equation. *Commun. Pure Appl. Math.* **36**, 291–324 (1983)
- Ponce, E., Ros, J., Vela, E.: Limit cycle and boundary equilibrium bifurcations in continuous planar piecewise linear systems. *Int. J. Bifurc. Chaos* **25**, 1530008 (2015)
- Ponce, E., Ros, J., Vela, E.: The boundary focus-saddle bifurcation in planar piecewise linear systems. Application to the analysis of memristor oscillators. *Nonlinear Anal. Real World Appl.* **43**, 495–514 (2018)

37. Rinzel, J.: Repetitive activity and Hopf bifurcation under point-Stimulation for a simple FitzHugh–Nagumo nerve conduction model. *J. Math. Biol.* **5**, 363–382 (1978)
38. Strukov, D.B., Snider, G.S., Stewart, D.R., Williams, R.S.: The missing memristor found. *Nature* **453**, 80–83 (2008)
39. Wang, J., Huang, C., Huang, L.: Discontinuity-induced limit cycles in a general planar piecewise linear system of saddle-focus type. *Nonlinear Anal. Hybrid Syst.* **33**, 162–178 (2019)
40. Yao, P., Wu, H., Gao, B., Tang, J., Zhang, Q., Zhang, W., Yang, J.J., Qian, H.: Fully hardware-implemented memristor convolutional neural network. *Nature* **577**, 641–646 (2020)
41. Zhang, Z., Ding, T., Huang, W., Dong, Z.: *Qualitative Theory of Differential Equations*, Transl. Math. Monogr., Amer. Math. Soc., Providence, RI (1992)

Publisher's Note Springer Nature remains neutral with regard to jurisdictional claims in published maps and institutional affiliations.

Springer Nature or its licensor (e.g. a society or other partner) holds exclusive rights to this article under a publishing agreement with the author(s) or other rightsholder(s); author self-archiving of the accepted manuscript version of this article is solely governed by the terms of such publishing agreement and applicable law.